von KARMAN INSTITUTE

FOR FLUID DYNAMICS

TECHNICAL NOTE 87

GRANTS AFOSR 71-2147 and 71-2147A

Interim Scientific Report
72 May 01 - 73 April 30

EFFECT OF SHOCK IMPINGEMENT ON HEAT TRANSFER

Jean J. GINOUX and Richard D. MATTHEWS

MAY, 1973

This research has been sponsored in part by the Air Force Office of Scientific Research, under Grants 71-2147 and 71-2147A.

RHODE SAINT GENESE BELGIUM

von KARMAN INSTITUTE FOR FLUID DYNAMICS

TECHNICAL NOTE 87

GRANTS AFOSR 71-2147 and 71-2147A

Interim Scientific Report
72 May 01 - 73 April 30

EFFECT OF SHOCK IMPINGEMENT ON HEAT TRANSFER

Jean J. GINOUX and Richard D. MATTHEWS

MAY, 1973

This research has been sponsored in part by the Air Force Office of Scientific Research, under Grants 71-2147 and 71-2147A.

ABSTRACT

The static pressure and heat transfer rate distributions have been measured in the reattachment region of free shear layers. In the first part, a cone/cavity model and the effects of gas injection have been studied. Results have been presented for both laminar and turbulent flows.

In the second part, a flow model has been investigated which is analogous with an Edney type III shock wave interaction, found when the bow shock of a blunt hypersomic body is intersected by an extraneous shock.

TABLE OF CONTENTS

1. GENERAL INTRODUCTION

This report contains the details and results of two experiments carried out at the von Karman Institute. They are related in that they are both concerned with pressure and heat transfer distributions in the reattachment region of free laminar and turbulent shear layers.

The first part of the report deals with a cone/cavity flow investigation in which conditions at reattachment are modified by gas injection into the cavity. Results for turbulent shear layers are presented and compared with previously obtained laminar data. Some correlations are suggested and discussed.

The second part of the report contains the experimental details and the results of an investigation made at the reattachment point of a two-dimensional shear layer of zero initial thickness.

Edney (Ref. 25) has discussed the high heat transfer rates found on blunt hypersonic bodies under circumstances in which its bow shock is intersected by an extraneous shock. This shock intersection produces a shear layer, and it is the impingement of this shear layer on the body surface which produces very high heat transfer peaks. The aim of this experiment is to reproduce the essentials of a steady two dimensional shock wave interaction.

2. TURBULENT CONE-CAVITY FLOW - THE EFFECTS OF GAS INJECTION

2.1 Introduction

The flow separation caused by a cavity on the surface of a hypersonic body considerably modifies the surface distributions of static pressure and heat transfer rate in that region. Whilst in the separated region itself these quantities are changed in an acceptable way, peaks well above the undisturbed values of both pressure and heat transfer rate have been measured as the flow reattaches (Refs. 1, 4, 6, 7).

It has been shown theoretically and verified experimentally that the injection of a small amount of gas into the cavity will substantially reduce these peaks. These investigations have been carried out in both the laminar regime (Ref. 2, 5, 8, 9, 10) and the turbulent regime (Ref. 11, 12, 13, 14, 17, 18, 23).

Ginoux and Thiry (Ref. 2) have verified that in the case of laminar cone/cavity flows the injection of gases which are lighter than the primary fluid are more effective in reducing the peaks. The subject of the present report is an extension of this work into the turbulent regime, using essentially the same equipment. The experimental program was carried out by Miss J. Yhap (Ref. 26). Results of static pressure and heat transfer surveys are presented and compared with the results of the earlier laminar tests.

2.2 Experimental equipment

2.2.1 Wind tunnel

The investigation was carried out in the hypersonic blowdown wind tunnel H-1 at the von Karman Institute. The working section measured 12 cm × 12 cm and the free stream Mach

number was 5.3±0.025.

The tunnel stagnation pressures used were from 28.8 atmospheres to 31 atmospheres with stagnation temperatures between 160°C and 220°C. These conditions gave free stream unit Reynolds numbers in the range of 3.28 to 4.04×10^5 per centimeter.

2.2.2 Models

The models used in this series of tests are identical with the models used by Ginoux and Thiry in reference 2 with the exception that the present models possess roughened noses so that the boundary layer becomes turbulent prior to separation. The roughnesses have the form of small steps on the forecone and details of these are shown in Fig. 1.

Two models were used, one for pressure measurements and the other for heat transfer studies. Their geometries differ slightly as shown in Fig. 2 and Fig. 3. The pressure measurement model has twenty eight static pressure tappings. Tapping number one on the forecone measures the cone pressure to which all pressures are referred. Numbers two and three are in the cavity whilst the distribution of the remainder is shown in Fig. 2.

The heat transfer model is fitted with eleven thermocouples as shown in Fig. 3. Thermocouple number 14 measures the reference heat transfer rate downstream of the cavity. Thermocouples numbered 9, 10 and 12 have been previously removed.

Both the static pressure tappings and the thermocouples are staggered by an angle θ to allow a very detailed examination to be made in the shear layer reattachment region.

2.2.3 Gas injection system

Four gases, including air, were used as injectants

during the tests. Two of them were lighter than air : hydrogen and helium, and one was heavier than air, namely, freon 12. No heat transfer measurements were taken for hydrogen injection.

The gases were injected through an annular port in the cavity at floor level as shown in Fig. 2 and Fig. 3. A diagram of the injection system is shown in Fig. 4. The gas metering was precisely carried out by using calibrated sonic orifice plates. This calibration was done by measuring the time between successive levels of pressure and temperature in a tank of known volume downstream of the orifices. A constant reservoir pressure was maintained upstream of the orifice plates.

Careful design of the model's interior produced variations of entry velocity into the cavity of less than 1%. The injectant mass flow rates were referred in both the laminar case and the turbulent case to the theoretical mass flow contained in the boundary layer at separation. Thus the normalized injectant mass flow is

$$C_q = \frac{Q_{inj}}{Q_{BL}}$$

where Q_{inj} = injectant mass flow rate

Q_{BL} = boundary layer mass flow at separation point

2.2.4 Model alignment

The model was initially set at zero degrees yaw and incidence related to the tunnel datum. This had to be adjusted very slightly so that a uniform annular pressure distribution was obtained at the reattachment shoulder.

2.2.5 Heat transfer measurements

Heat transfer measurements were made using the transient thin skin technique. This utilizes the equation which gives the heat transfer to the surface per unit area and time and is written as :

$$\dot{q} = \rho c d \frac{\partial T}{\partial t}$$

where ρ skin density = 7.68 gm/cm^3
c specific heat = 0.114 cal/gm°K
d effective skin thickness

During the experiment the tunnel was started very quickly, the model being initially at a uniform temperature. The slope $\frac{\partial T}{\partial t}$ of the temperature-time graph was measured at a very small time after starting the tunnel. At this time, ideally the model is still at a uniform temperature and therefore little conduction will be taking place within it.

2.3 Results and discussion

2.3.1 Flow visualization results

Photographs of the flow past the cone/cavity model were obtained using the shadowgraph technique. These are shown in Figs. 5a to 5m.

The flow regime shown in Fig.5a is for zero mass injection. In this photograph, there is evidence of an expansion fan at the separation point and an oblique shock emanating from the reattachment region. Measurements reveal that the cavity pressure is below the cone pressure for zero mass injection.

The particular circumstances governing the flow over a cavity having flush lips have been described in the literature (Chapman, et al.) as the following.
The flow regime is governed by two effects. Firstly, the shear layer has a scavenging effect upon the air in the cavity and therefore tends to exert a suction upon it. Secondly, the shear layer reattachment flow field must be such that it returns to the cavity that mass flow which has been entrained by the shear layer. The equilibrium condition in this particular experiment is one in which the suction has caused the shear layer to be

expanded slightly at separation with the consequent abrupt reattachment at the shoulder causing the oblique shock shown in Fig.5a.

This flow regime is modified by the injection of gas into the cavity. In Figs. 5b and 5c, the injectant is air. At low injectant mass flow rates shown in Fig. 5b and 5c, there is no discernable alteration in the flow structure. However, as the mass flow rate is increased further, (Fig. 5d), there is evidence of a compression wave emanating from the separation point, and a weakening of the oblique shock at the reattachment shoulder. This trend is continued in Fig. 5e with a definite compression wave at separation and a much weaker compression wave at the reattachment point.

The shadowgraphs shown in Fig. 5f to Fig.5i are for the freon 12 injection case. The information contained in them infers that, for the same injection rates, the freon 12 does not produce the flow field modifications which were caused by air. For example, even at the highest rate of freon 12 injection there is only a slight trace of a compression wave at the separation corner.

On the other hand, the helium injectant produces marked alterations to the flow field even at very low mass flow rates as shown by the series of shadowgraphs in Figs. 5j to 5m . It is apparent that helium mass flow ratios of 0.05 are sufficient to weaken the reattachment compression wave, whilst for a c_q value of 0.131 the rear compression wave is standing well off the body with the separation compression wave well defined. In Fig. 5m the separation wave is even more intense with a grazing type of reattachment being indicated at the shoulder.

The results of the shadowgraph examination for the turbulent shear layer exhibit the same trends as the laminar results of Ginoux and Thiry (Ref. 2) in that again the lighter

gases seem much more efficient at lifting the shear layer off the reattachment shoulder which of course leads one to expect reduced levels of static pressure and heat transfer in that region.

2.3.2 Pressure and heat transfer measurements

The results of this part of the investigation are presented initially in the form of graphs showing the distribution of static pressure ratio along the model surface. The effects of injecting the various gases is shown in Fig. 6 to Fig. 9. In all these figures the effect of mass injection is to reduce the pressure levels leaving the form of the distribution unaltered.

In studying these four figures, it is obvious that the lighter gases are able to reduce the pressure levels at reattachment for very small injectant mass flows. This effect is illustrated in Fig. 10, in which the peak pressure, after being normalized with respect to the peak pressure for zero injection, is plotted against c_q. The laminar results have also been plotted on this figure; it should be remembered, however, that the reference mass flow for calculating c_q is different in the laminar case.

A study of the shadowgraphs in conjunction with Fig. 10 leads to the conclusion that the reduction in the reattachment peak pressure is associated in some way with the shear layer angular displacement. The cavity pressure is a measure of this movement and so the way in which the cavity pressure is affected by the various injectants should be examined.

In figure 11 the effect of injectant mass flow on the cavity pressure is shown for turbulent and laminar flow. At zero injectant mass flow rate, the cavity pressure in the turbulent case is well below that for the laminar regime.

This may be due to the fact that the much higher mass flow entrainment rates associated with turbulent free shear layers exert a higher suction on the contents of the cavity than the laminar shear layers, so that the equilibrium flow regime in the turbulent case will involve larger expansion angle at separation than in the laminar case and, consequently, more severe pressure rise at reattachment to return to the cavity the high mass flow which has been entrained by the turbulent shear layers.

The curves on Fig. 11 show, as expected, that the cavity pressure is highly dependent on the type of injectant and in both laminar and turbulent regimes, it is the light gases which have the strongest effect on the cavity pressure.

The injectant mass flows for both the laminar and the turbulent regimes have been referred to the mass flow in the turbulent boundary layer at separation. Plotting the results in this way illustrates the difference in the sensitivities of the laminar and turbulent regimes to the injectant mass flow.

Examination of Figs. 6 to 9 in conjunction with Fig.11 leads to the conclusion that the peak pressure at reattachment will be a function of the reattachment angle which in turn reflects the cavity pressure.

The reattachment pressure peak should then be a unique function of the cavity pressure. By correlating the peak pressure and later the peak heating with the cavity pressure the dependence on the injectant type is removed. Figure 12 shows this type of correlation to be a reasonable one. By again recalling the laminar results of Ref. 2, the reattachment pressure peaks can be plotted against the cavity pressure as shown in Fig. 13.

Both these figures show excellent correlation for cases in which the shear layer is expanding down into the cavity. As the cavity pressure increases the shear layer tends to graze

the reattachment shoulder and consequently the peak pressures decrease. However, once the cavity pressure exceeds the cone pressure the shear layer starts to lift off the reattachment shoulder so that the peak pressure looses its dependence on shear layer angular direction and the cavity pressure. This trend is reflected in both Figs. 12 and 13. The line drawn on both figures labelled $P_{max} = P_{cav}$ is of course a limiting line.

The results of the heat transfer survey are shown in Figs. 14 to 16. They are in the form of surface heat transfer rate measured on the cone surface far downstream of the cavity. These figures show that the effects of gas injection on the heat transfer distributions are similar to the effects produced by gas injection on the static pressure distribution. The general form of the distributions is unchanged but the levels are progressively reduced with increasing injectant mass flow.

The effect of the various injectants on the peak value of heat transfer is shown in Fig. 17. The efficiency of the lighter gases is shown clearly.

The dependence of the peak heating on the reattachment angle is shown by plotting the peak heating against the cavity pressure. Figure 18 shows this type of correlation in the turbulent regime to be very good. However, the laminar results plotted in Fig. 19 only correlate against the cavity pressure whilst the cavity pressure ratio is less than unity. Once the cavity pressure exceeds the cone pressure, the heat transfer peak is below the reference value. Under these conditions, the results of Ref. 2 show that the flow becomes transitional downstream of the reattachment shoulder where upon the heat transfer rates rise sharply.

To examine the results in greater detail, it is interesting to study the relationship between the peak heating and the peak pressure for both the turbulent and laminar regimes.

The results plotted in this way are shown in Figs. 20 and 21.

Both the laminar and the turbulent results show a linear relationship between the peak pressure and the peak heating for the cases in which the cavity pressure is below the cone pressure. These are the high heat transfer cases.

By defining a maximum reattachment Stanton number in a similar way to Bushnell and Weinstein (Ref. 27) based on the peak heating, the peak pressure and the wall temperatures such that

$$St_{max} = \frac{\dot{q}_{max}}{\frac{P_{max}}{R\,T_w}\,u\,c_p(T_0-T_w)}$$

where u is the velocity just downstream of the oblique shock which for shallow reattachment angles is approximately equal to the cone velocity.

The reference Stanton number is thus written as

$$St_{ref} = \frac{\dot{q}_{ref}}{\frac{P_{cone}}{R\,T_w}\,u_{cone}\,c_p(T_0-T_w)}$$

with $u_{cone} \simeq u$

so that

$$\frac{\dot{q}_{max}}{\dot{q}_{ref}} = \frac{St_{max}\,P_{max}}{St_{ref}\,P_{cone}}$$

The linear portions of Figs. 20 and 21 are of course of the form

$$\frac{\dot{q}_{max}}{\dot{q}_{ref}} = m\,\frac{P_{max}}{P_{cone}} + c$$

or

$$\frac{St_{max}}{St_{ref}} = m + c\,\frac{P_{cone}}{P_{max}}$$

for turbulent shear layer $m = 3.07$
$c = -4.81$
for laminar shear layer $m = 2.21$
$c = -1.915$

The laminar and the turbulent results are plotted in this way in Fig. 22, with the values at zero injectant rate indicated as well as the point at which the cavity pressure is equal to the cone pressure.

St_{ref} is different for each case so that the vertical position of the curves will depend upon the chosen reference Stanton number. Nevertheless, it is seen that the dependence of the maximum Stanton number on the peak pressure is of the same order in both the laminar and the turbulent regimes.

A correlation factor K was calculated in a similar manner to Ref. 2, in an attempt to collapse the peak pressure and peak heat transfer curves onto the curve for the air injection case (see Fig. 23). The correlation factor K is related to the molecular weight of the injectant as shown in Fig. 24. This correlation was successful in the laminar case but is not so effective for the turbulent case as shown by the scatter in Fig. 24. This is possibly due to the fact that the diffusion processes in the laminar case are only dependent on the molecular weight whereas of course in the turbulent case the diffusion is done by the eddies within the flow.

The distributions of heat transfer and static pressure for zero injectant mass flow for the turbulent and laminar results are shown in Fig. 25. In the laminar flow case the heat transfer peak occurs downstream of the static pressure peak. On the other hand, for the turbulent shear layer, the heat transfer peak is upstream of the static pressure peak. In both cases, the heat transfer is related to the static pressure through the density; in the laminar case the acceleration downstream of the pressure peak increases the wall temperature gradient, whilst in

the turbulent case the flow acceleration downstream of the pressure peak may be tending to laminarize the boundary layer and consequently reducing the heat transfer rate.

When setting the pressure model to zero incidence, during the laminar flow experiments, it was noticed that the annular pressure distributions on the reattachment shoulder were extremely sensitive to the model incidence, with very large pressure differences between the windward and leeward sides. These pressure differences were apparent for incidences of $\frac{1}{2}$ ° upwards. On the other hand, during the turbulent tests changes of incidence of up 2° produced very little change in the annular pressure distribution.

2.4 Conclusions

Measurements of static pressure and heat transfer rate on the cone-cavity model used in Ref. 2 have been made in the turbulent regime.

Injection of gases into the cavity have caused the pressure there to rise and substantially reduce the peak pressure and peak heat transfer rate in the reattachment region.

As in Ref. 2, the lighter gases have proved most efficient in this respect.

When the cavity pressure was below the cone pressure a linear correlation was found between the peak heat transfer rate and the peak pressure at reattachment in both the laminar and turbulent regimes. Using a reattachment Stanton number definition proposed by Bushnell and Weinstein in Ref. 27, it was found that the maximum Stanton number at reattachment, referred to some reference value, showed the same dependence on the peak pressure in both the laminar and the turbulent flow regimes.

3. REATTACHING SHEAR LAYER INVESTIGATION

3.1 Introduction

Very high levels of heat transfer rate have been measured on the forward surfaces of blunt hypersonic bodies in the reattachment region of a shear layer. This shear layer is generated by the intersection of the bow shock and an extraneous oblique shock. Such a situation may occur when the bow shock of a shuttle type vehicle intersects the bow shock generated by its booster.

Edney, in Ref. 25, distinguishes between six different types of shock intersection and discusses the conditions under which each may occur. Edney's type III intersection results in very high peak values of heat transfer at the point where a shear layer generated by the intersecting shocks, attaches to the surface of the body. Under type III conditions, the shear layer separates a subsonic region near the body from a supersonic region which, for most free stream Mach numbers of interest, is between 2.0 and 3.0.

The experiment described in this report is concerned with measurements of static pressure and heat transfer rate on the surface of a cylinder at the impingment point of such a shear layer having zero initial thickness. Laminar and turbulent shear layers have been studied.

3.2 Experimental equipment

3.2.1 Wind tunnel

The experiment was carried out in the VKI supersonic wind tunnel S-1. This is a closed circuit wind tunnel with a working cross sectional area measuring 40 cm by 40 cm. The nominal free stream Mach number is 2.21. During the tests the stagnation pressure was varied between 80 and 190 mm Hg.abs. with stagnation

temperatures between 295°K and 310°K. These gave a unit Reynolds number range of between 1.3×10^6 and 3.1×10^6 per meter.

3.2.2 Model

The model consists of a shear layer generator fixed upstream of a horizontal cylinder perpendicular to the free stream which is 6 mm diameter and 250 mm long. The arrangement is shown diagramatically in Fig. 26 and a photograph of the model is shown in Fig. 27. The cylinder can be rotated about its axis through any angle. A single static pressure tapping is used to measure the static pressure distribution in the reattachment region of the shear layer.

The pressure tapping is connected to a Statham differential pressure transducer of the strain gauge type having a range of 0 to 1.0 lbf/in^2. The signal from the transducer is displayed on a graphispot chart recorder.

The heat transfer rate distribution in the reattachment region is found using the transient thin skin technique wih with a single copper/constantan thermocouple. This technique was described in section 2.2.2 of the first part of this report. Prior to each test a 0.2 KW heater is placed around the cylinder which gives it a uniform temperature of about 100°C. Pneumatic jacks quickly move the heater along the cylinder away from the region of interest at the beginning of each test.

The cylinder and the shear layer generator can be moved relative to each other to produce different reattachemnt configurations. The analogy between the experimental set up and an Edney type III interaction is shown in Fig. 28.

The correspondance between the experimental set up in Fig.28b and the real situation in Fig. 28a is as follows First of all, obviously the Mach number above the shear layer labelled M_2 in the Edney report corresponds with M_1 in the

experiment. The Mach number below the shear layer in the real situation is M_3 which is subsonic ($M_3 \simeq 0.4$) where as in the model there is a cavity flow. Edney refers all the static pressure measurements to the total pressure P_{20} behind a normal shock at the free stream Mach number. Again the analogy assumes that since $M_3 << 1.0$ the static pressure is approximately equal to the total pressure so that the cavity pressure on the model corresponds to P_{20}. Unfortunately, the cavity pressure is not constant for different geometries where as Edney's P_{20} only depends on the free stream Mach number. Consequently, since with the model, the cavity pressure was approximately equal to the free stream static, all pressures were referred to this.

The analogy extends to the heat transfer measurements of course. In the Edney report the heat transfer measurements have been normalized with respect to the stagnation point heat transfer rate at the free stream Mach number. By assuming that the shear layer had been generated by an Edney type III shock intersection it is possible to calculate an equivalent hypersonic free stream Mach number. By then assuming that the cavity static pressure, measured on the model, is equal to the total pressure of the flow on the subsonic side of the shear layer in the hypersonic interaction case, then the equivalent hypersonic free stream static pressure can be found. By assuming the same total temperature in both flows it is possible to calculate the equivalent flow Reynolds number. The equivalent hypersonic flow Reynolds number is $\frac{1}{2\delta}$ the Reynolds number of the flow used in the experiment.

From these calculations a stagnation point heat transfer coefficient in the equivalent hypersonic flow can be evaluated. The heat transfer measurements are referred to this value, q_{20}.

3.3 Results and discussion

3.3.1 Criterion for laminar/turbulent shear layer

The heat transfer rate is highly dependent upon whether the reattaching shear layer is laminar or turbulent. Experiments were to be carried out in both these regimes and it was therefore necessary to examine the flow carefully to distinguish between these regimes.

This was done by using a criterion developed by Ginoux (Ref. 28) in conjunction with shadowgraphs. The criterion is based on the fact that a separated region in laminar flow increases in size as the Reynolds number is increased. As the Reynolds number is increased further and transition occurs the separated length decreases sharply. Finally, when the Reynolds number reaches a high enough value, the flow becomes completely turbulent and the separated length increases again. Thus a pressure tapping suitably placed in the separate region can be related to the separated length and hence the flow regime, as shown in Fig. 29 .

During the experiment the static pressure tapping was on the cylinder in the reattachment region so that it corresponds to the pressure tapping P_2 in the explanatory diagram of figure 29 .

The Reynolds number of the shear layer was varied by changing the tunnel stagnation pressure and the distance between the shear layer generator and the cylinder.

The results of this part of the investigation are shown in Fig. 30 . The static pressure trends in the reattachment region are clearly shown and are in agreement with the predictions made by Ginoux in reference 28. The evidence shown in figure 30 enables the measurements made later in the main body of the tests to be definitely labelled laminar or turbulent.

3.3.2 Flow visualization

Two photographs of the flow using the shadowgraph technique are shown in Fig. 31. In Fig. 31a an obviously laminar shear layer is shown reattaching to the surface of the cylinder. The reattachment is of the grazing type but even so a weak oblique shock can be seen emanating from the reattachment region.

The photograph of Fig. 31b illustrates a typical turbulent flow configuration. The double image of the oblique shock at reattachment is caused by the span effect.

For the laminar tests the shear layer remained substantially straight, and reattachment occurred high up on the cylinder producing a weak oblique shock. To obtain a turbulent shear layer, the length L, had to be doubled to produce the necessary Reynolds number as shown in Fig. 31b. Because of this the shear layer tended to reattach to the cylinder at more abrupt angles than the laminar shear layer. This produced in some cases strong oblique shocks of the bow shock type at reattachment.

3.3.3 Static pressure and heat transfer distributions

Three model geometries were tested in the laminar flow regime, with the vertical cylinder displacement $\frac{h}{R}$ = 0, 0.33 and 0.635. The length L was fixed at 17.5 mm. Two runs were made in each case with the tunnel stagnation pressures set at approximately 80 mm Hg and 100 mm Hg. The pressure distributions are shown in Fig. 32. The static pressure measurements have been referred to the free stream static pressure. All three sets of test points illustrate the same trend, i.e., low pressure at $\theta = 0$, which is approximately equal to the cavity pressure, the pressure then rises to some peak value in the shear layer reattachment region before falling again towards $\theta = 90°$.

The pressure peak itself is increasing in size and moving around the cylinder as $\frac{h}{R}$ is increased. Two lines have been added to Fig. 32 to try and give a certain amount of perspective to the measured values. The first of these lines is plotted in an attempt to relate these results to Fig. 5.9 and Fig. 5.12 of the Edney report. It shows the theoretical maximum pressure rise, calculated in the same manner as Edney, i.e., once the Mach number (M > 1) of the flow above the shear layer is known then an oblique shock pressure rise can be related to the local cylinder surface inclination. Measurements with a pitot probe above the shear layer suggest that the Mach number there to be approximately 1.95.

The static pressure rise through a normal shock at M = 1.95 has also been plotted in Fig. 32 .

The results of the heat transfer rate survey are shown in Fig. 33 . The test points have been omitted for clarity, the scatter is about $\pm$ 10%.

By referring both the static pressure distributions and the heat flux distributions to quantities which themselves were a function of free stream Reynolds number, then the effect of the Reynolds number on the results tends to be masked.

The heat transfer distribution about a cylinder in uniform flow at the equivalent hypersonic Mach number and Reynolds number has also been shown for comparison. The effect of $\frac{h}{R}$ can be clearly seen, following the same trends as the static pressure distributions with the larger values of $\frac{h}{R}$, causing a more abrupt reattachment and higher peak values of static pressure and heat transfer rate.

The relative positions of the heat transfer and static pressure peaks are shown in Fig. 34; for these laminar results, the pressure peak occurs before the heat transfer peak as in the laminar cone cavity results shown on Fig. 25.

The static pressure distributions for the shear layer reattachment in the turbulent regime are shown in Fig. 35. These tests were done with $\frac{h}{R} = 0$ and $\frac{h}{R} = 0.33$, with L = 36 mm. Again the Reynolds number effect is masked by the choice of reference pressure.

In the shadowgraph examination it can be seen that the turbulent shear layer curves downwards slightly into the cavity. The pressure distributions in Fig. 35 confirm this impression since the peak pressure occurs at approximately $\theta = 55°$.

The heat transfer distributions for the turbulent regime are shown in Figs. 36 and 37. For both cases of $\frac{h}{R} = 0$ and $\frac{h}{R} = 0.33$, the heat transfer rate shows slight dependence on the Reynolds number. Test points have again been omitted for clarity. The scatter is about $\pm$ 10 % about the lines shown.

In the cone cavity results presented in the first part of this report it was observed that in the laminar regime the pressure peak occurred before the heat transfer peak and that in the turbulent regime the reverse was true. This reversal is observed in one case for the reattaching shear layer results. For $\frac{h}{R} = 0$ the heat transfer peak occurs at about 54° whilst the pressure peak also occurs at about 54°. With $\frac{h}{R} = 0.33$, however, the heat transfer peak is between 40° and 44° depending on the Reynolds number, whilst the pressure peak occurs at about 47°. The possible reasons for the different trends in the laminar and turbulent results were discussed in section 2.3.2.

Bushnell and Weinstein (Ref. 27) have correlated the peak heat transfer rates associated with the reattachment region of a ramp induced boundary layer separation in both the laminar and turbulent regimes.

The peak Stanton number is related to a Reynolds number based on the distance between reattachment and peak heating. The Stanton number and the Reynolds number being evaluated using local conditions. It is argued that the distance between reattach-

ment and peak heating in both laminar and turbulent flow is of the order of the incoming boundary layer thickness, the arrangement is shown diagrammatically in Fig. 1 of Ref. 27; so

$$x_p \equiv \frac{\delta_s}{\sin(\theta_f - \theta_s)}$$

and for laminar boundary layers

$$\frac{h_{max}}{\rho_w u_3 c_p} \alpha \left[\frac{\rho_w u_3}{\mu_w} \frac{\delta_s}{\sin(\theta_f - \theta_s)}\right]^{-0.5}$$

and for turbulent boundary layers

$$\frac{h_{max}}{\rho_w u_3 c_p} \alpha \left[\frac{\rho_w u}{\mu_w} \frac{\delta_s}{\sin(\theta_f - \theta_s)}\right]^{-0.2}$$

This type of correlation was highly successful for the experimental results dealt with by Bushnell and Weinstein.

In the present experiments in which reattachment occurs on a curved surface where the radius of curvature is small and the reattachment is of the grazing type the correlation no longer holds. In fact, the peak Stanton numbers for the laminar results of both the cone-cavity and the reattaching shear layer experiments are approximately half the value expected from a Bushnell and Weinstein type of correlation. On the other hand, the correlation underestimates the turbulent peak Stanton numbers.

There is thus experimental evidence that when the surface radius of curvature is small it has a strong influence on the peak heating in reattachment regions and it is proposed to examine this theoretically using an integral theory.

3.4 Conclusions

Detailed measurements of static pressure and heat transfer rate distributions have been made as a shear layer re-attaches to the surface of a cylinder. The shear layer generator/cavity/cylinder combination have exhibited the same characteristics as those found by Edney for a type III shock wave interaction. By drawing an analogy between the model cavity pressure and the total pressure behind a normal shock at a hypersonic free stream condition, the peak pressures measured on the cylinder show the same trends and levels as found by Edney to exit for type III interactions.

Edney found that there existed a correlation between the peak heating and the peak pressure for a type III interaction of the form

$$\frac{q_{peak}}{q_{20}} = A\left(\frac{P_{peak}}{P_{20}}\right)^{1.35}$$

and for $M_\infty = 7.0$ $\quad A = 1.1$

$M_\infty = 4.6$ $\quad A = 2.2$

with the present results

$M_\infty = 2.21$ $\quad A = 2.4$ $\quad$ and the index is 0.32.

The turbulent results are difficult to correlate in this way since for at a given peak pressure the heat transfer peak value was highly dependent on the Reynolds number.

REFERENCES

1. CHAPMAN, D.R.: A theoretical analysis of heat transfer in regions of separated flows.
NACA TN 3972, 1956.

2. GINOUX, J.J. and THIRY, F.: Cone cavity flow at M = 5.3 with injection of light, medium and heavy gases.
VKI TN 35, November 1968.

3. GINOUX, J.J. and THIRY, F.: Cone cavity flow at M = 5.3 with injection. Effect of incidence.
VKI TN 75, June 1971.

4. NICOLL, K.M.: A study of laminar hypersonic cavity flow.
AIAA J., Vol. 2, Nr 9, pp 1535-1541, September 1964.

5. NICOLL, K.M.: Mass injection in a hypersonic cavity flow.
ARL 65-90, May 1964.

6. NICOLL, K.M.: An experimental investigation of laminar hypersonic cavity flows. Part II - Heat transfer and recovery factor measurements.
ARL 63-73, January 1964.

7. LARSON, H.K.: Heat transfer in separated flow.
J.A.S., Vol. 26, pp 731-738, November 1959.

8. FAULDERS, C.R.: A note on laminar boundary layer skin friction under the influence of foreign gas injection.
J.A.S., vol. 28, Febr. 1961, Reader's Forum, pp166-167.

9. ALBACETE, L.M. and GLOWACKI, W.J.: Skin friction and heat transfer characteristics of the compressible laminar boundary layer with injection of a light, medium and heavy gas.
NOL TR 66-215, March 1967.

10. CRAVEN, A.H.: The compressible laminar boundary layer with foreign gas injection.
CoA Report No 155, January 1962.

11. RUBESIN, M.W. and PAPPAS, C.G.: An analysis of the turbulent boundary layer characteristics on a flat plate with distributed light-gas injection.
NACA TN 4149, February 1958.

12. PAPPAS, C.C. and OKUNO, A.F.: Measurement of heat transfer and recovery factor of a compressible turbulent boundary layer on a sharp cone with foreign gas injection.
NASA TN D 2230, April 1964.

13. FOGAROLI, R.P. and SAYDAH, A.R.: Turbulent heat transfer and skin friction measurements on a porous cone with air injection at high Mach numbers.
AIAA J., vol. 4, Nr 6, p 1116, June 1966.

14. POLEK, T.E. and G.G.: Measurements of turbulent heat transfer on cones and swept plates at angle of attack.
NASA SP 216, 1969

15. MORRISETTE, E.L., STONE, D.R., CARY, A.M.: Downstream effects of boundary layer trips in hypersonicfflow.
NASA SP 216, 1969.

16. REBUFFET, P.: Aérodynamique expérimentale. Tome 2.
Paris, Dunod, 1966.

17. PAPPAS, C.C. and OKUNO, A.F.: Measurement of skin friction of the turbulent boundary layer on a cone with foreign gas injection.
J.A.S., vol. 27, Nr 5, pp 321-333, May 1960.

18. CHARWAT, A.F.: An investigation of separated flows - Part 2, Flow in the cavity and heat transfer.
J.A.S., vol. 28, pp 513-527, 1961.

19. VAN DRIEST, E.R.: Turbulent boundary layers in compressible fluids.
J.A.S., vol. 18, Nr 3, pp 145-161, 1951.

20. BARTLE, R.E. and LEADON, B.M.: The compressible turbulent boundary layer on a flat plate with transpiration cooling. 1. Measurements of heat transfer and boundary layer profiles.
C.S.R.L. RR 11, May 1961.

21. BOGDONOFF, S.M. and VAS, I.E.: Some experiments on hypersonic separated flows.
ARS J., October 1962.

22. HOPKINS, E.J. and INOUYE, M.: An evaluation of theories for predicting turbulent skin friction and heat transfer on flat plates at supersonic and hypersonic Mach numbers.
AIAA J., vol. 9, Nr 6, pp 993, 1971.

23. NESTLER, D.E., SAYDAH, A.R., AUXER, W.L.: Heat transfer to steps and cavities in hypersonic turbulent flow.
AIAA J., vol. 7, Nr 7, pp 1368-1370, 1969.

24. HOLLOWAY, P.F., STERRET, J.R., CREEKMORE, H.S.: An investigation of heat transfer within regions of separated flow at Mach numbers of 6.
NASA TN D 3070, November 1965.

25. EDNEY, B.: Anomalous heat transfer and pressure distributions on blunt bodies at hypersonic speeds in the presence of an impinging shock.
FFA Report Nr 115, 1968.

26. YHAP, B.J.: Cone/cavity flow at M = 5.3 with mass injection. Turbulent boundary layer.
VKI Project Report 72-306, 1972.

27. BUSHNELL, D.M. and WEINSTEIN, L.M.: Correlation of peak heating for the reattachment of separated flows.
J. Spacecraft and Rockets, Sept. 1968, p. 1111.

28. GINOUX, J.J.: Supersonic separated flows over wedges and flares with emphasis on the method of detecting transition.
VKI TN 47, August 1968.

29. STOCK, H.: An approximate calculation of the laminar heat transfer in the stagnation region of spheres and cylinders in high speed flow.
VKI TN 84, October 1972.

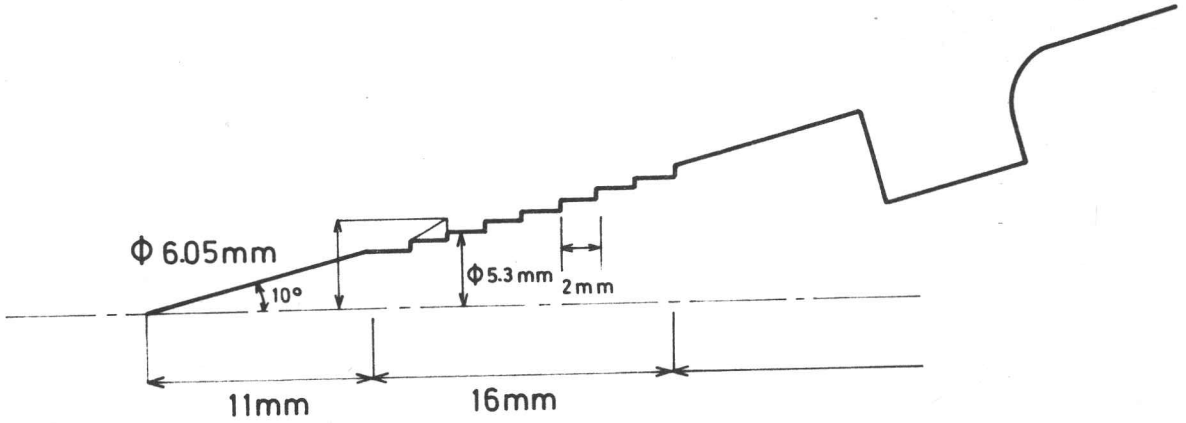

Fig.1 - DETAIL OF ROUGHNESS ON FORECONE.

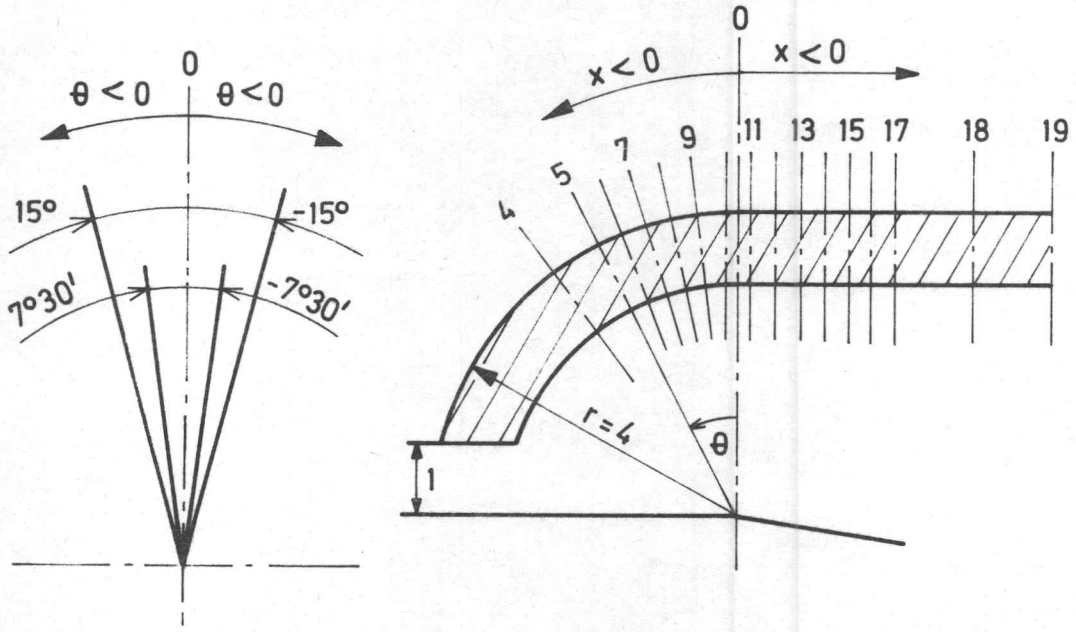

Fig. 2 - PRESSURE MODEL (Dimensions in mm.)

No.	x	θ
4	- 2.61	0
5	- 1.92	15
6	- 1.57	7°30
7	- 1.22	-7°30
8	- 0.87	-15
9	- 0.54	15
10	- 0.18	7°30
11	0.18	-7°30
12	0.48	-15
13	0.78	15
14	1.08	7°30
15	1.38	-7°30
16	1.68	-15
17	2.50	0
18	3.18	0
19	4.14	0
20	11.14	0

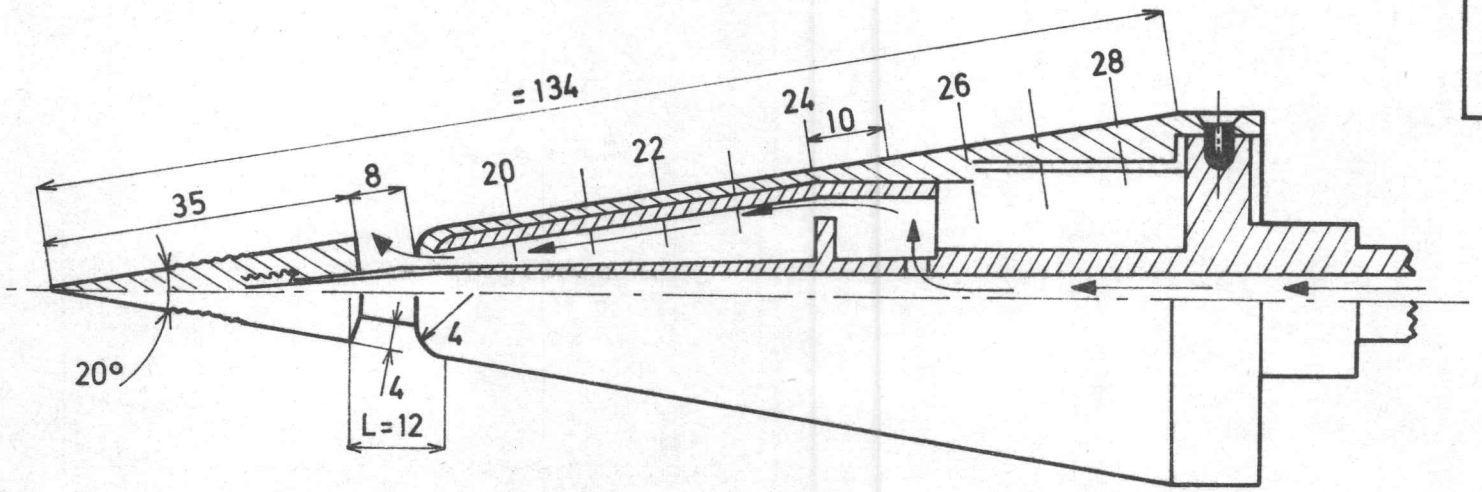

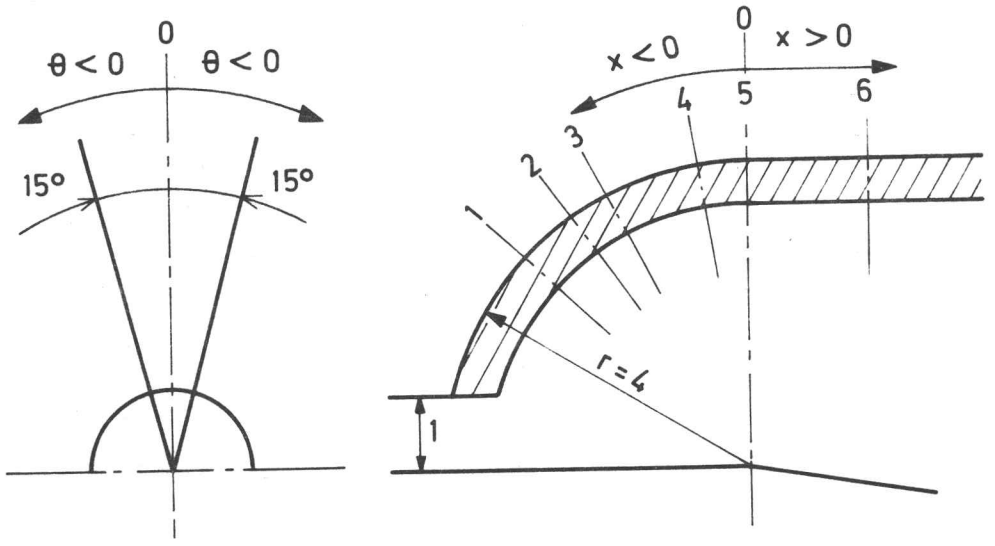

No.	x	θ
1	- 3.30	15
2	- 2.49	0
3	- 1.99	-15
4	- 0.69	15
5	0	0
6	1.59	0
7	3.20	0
8	7.99	0
11	13.20	0
13	23.10	0
14	36.36	0

Fig. 3 - HEAT TRANSFER MODEL (Dimensions in mm.)

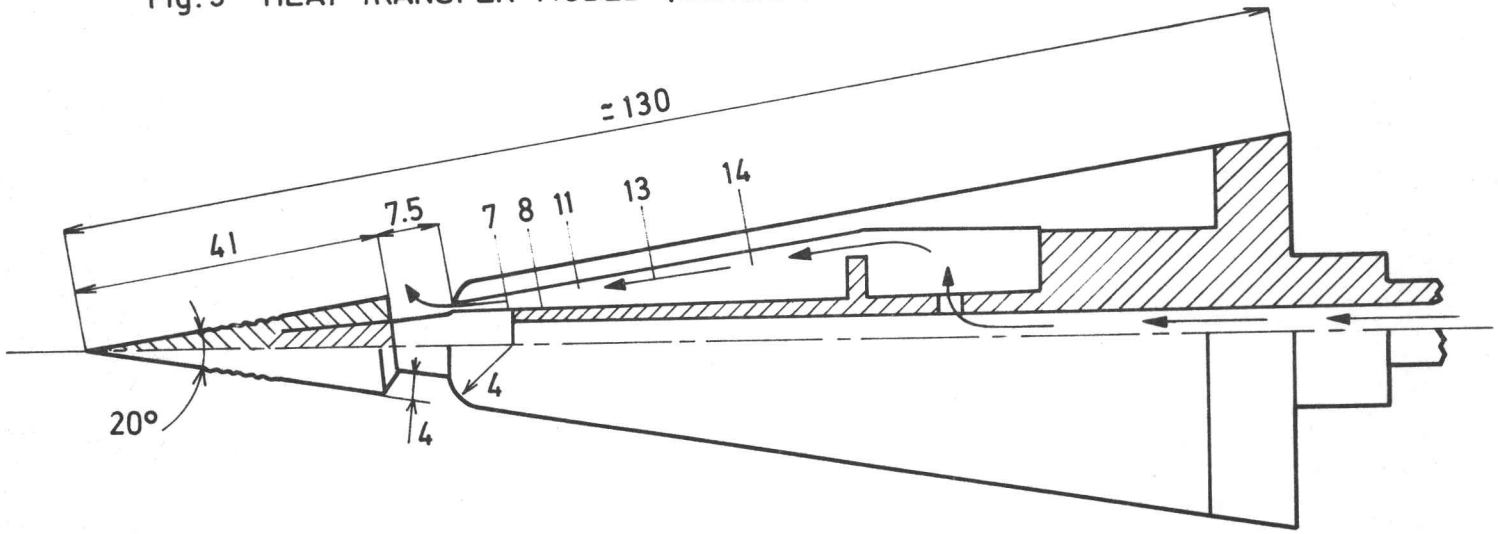

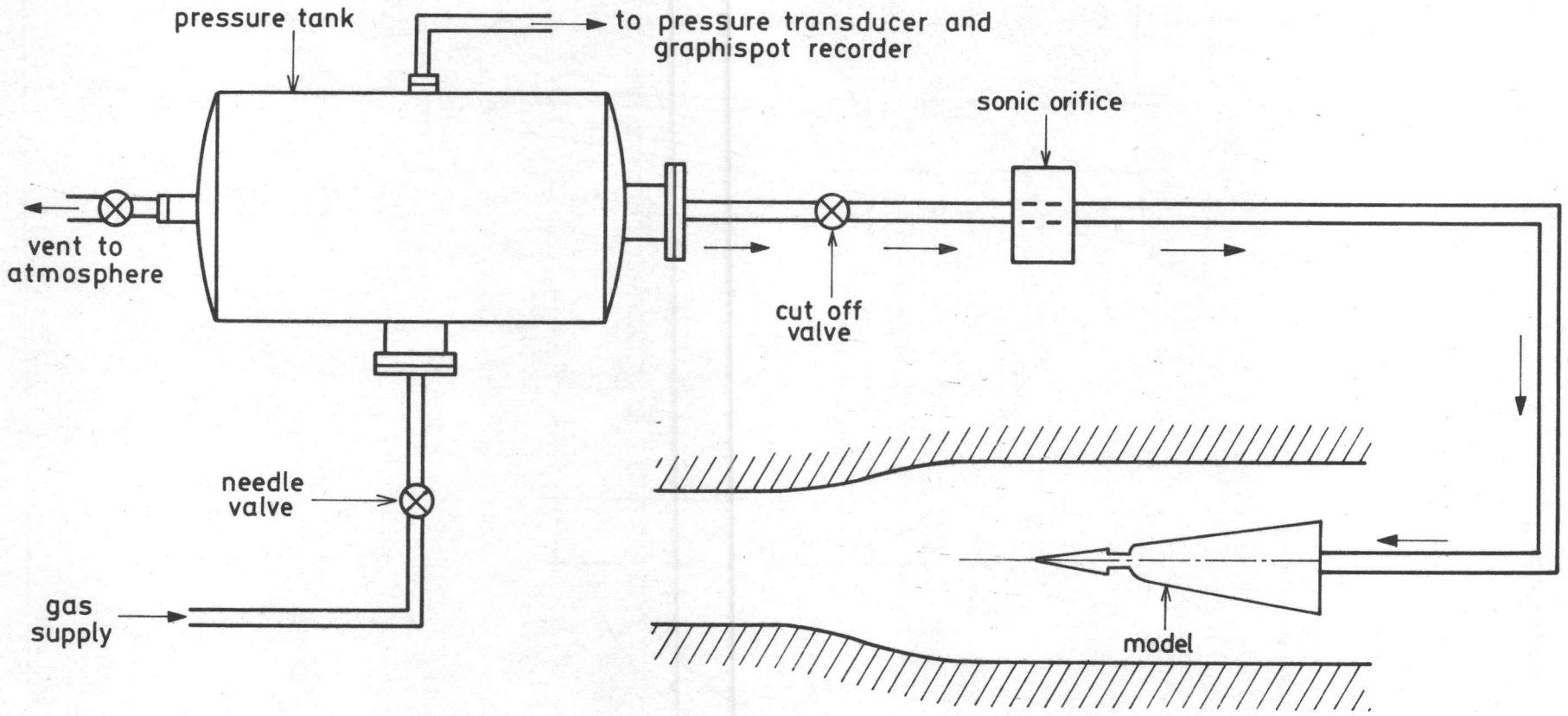

Fig. 4 - GAS INJECTION SYSTEM

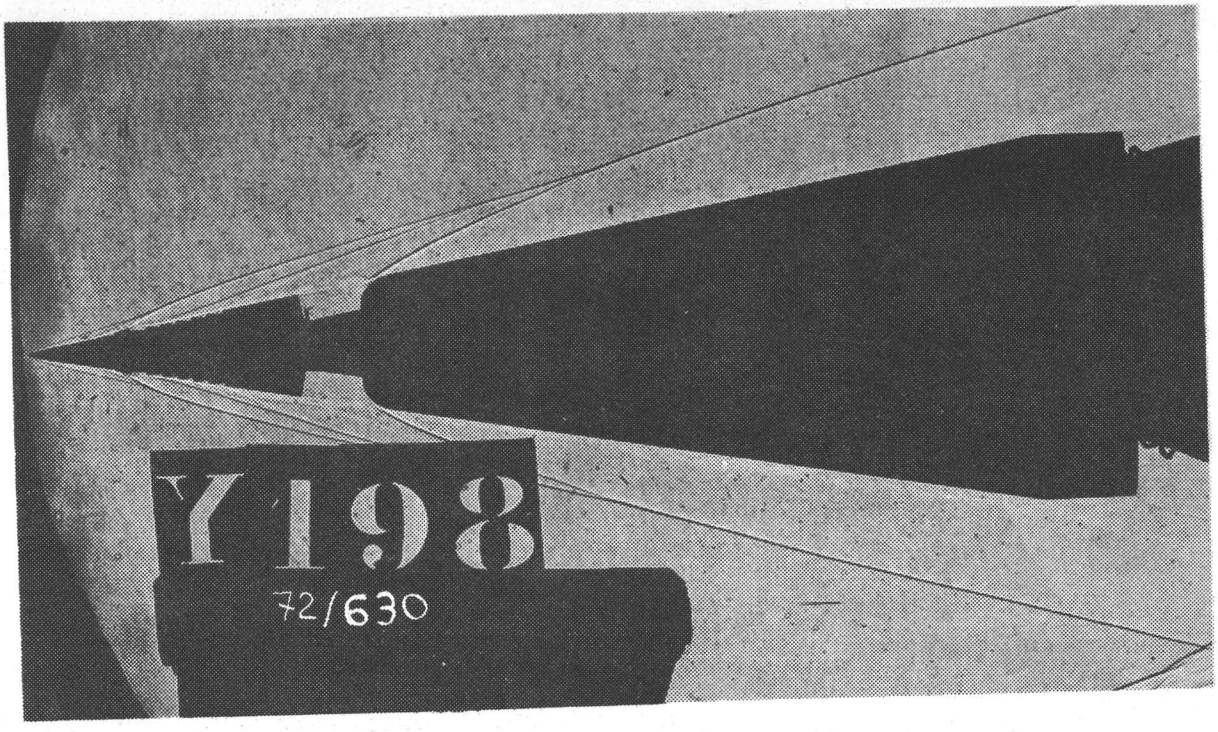

Fig. 5 (a) - SHADOWGRAPH OF CONE/CAVITY FLOW. ZERO INJECTION.

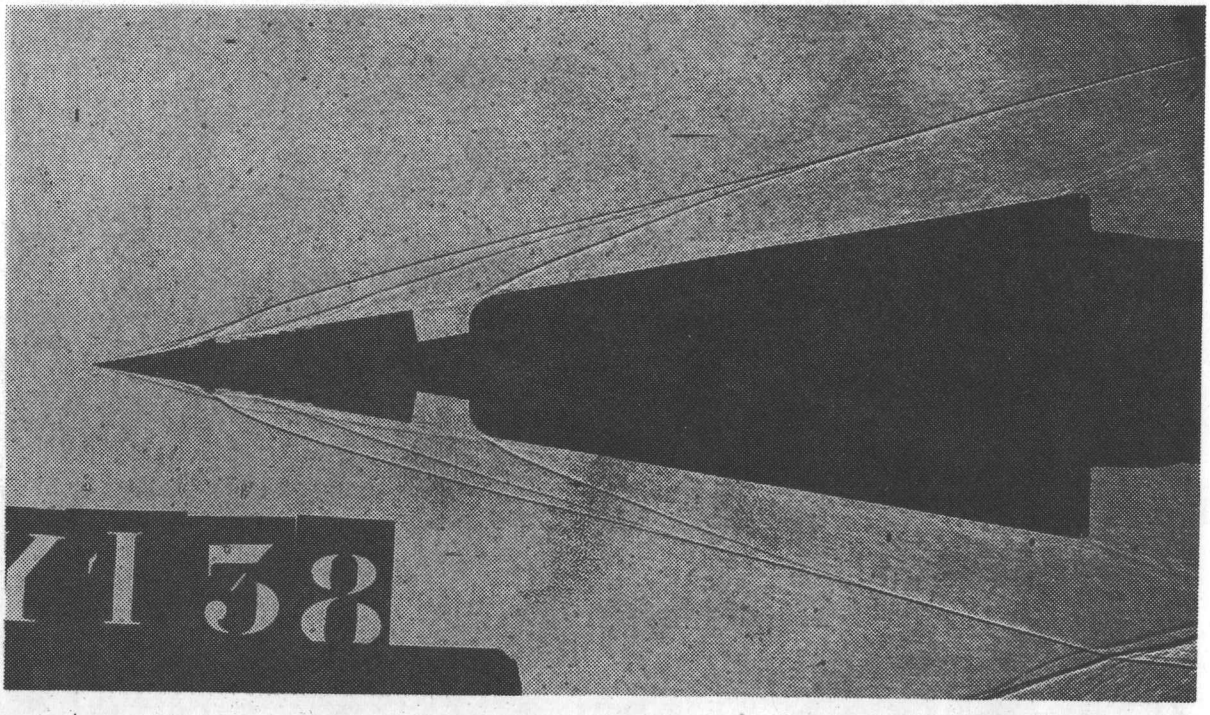

Fig. 5 (b). C_q = .041

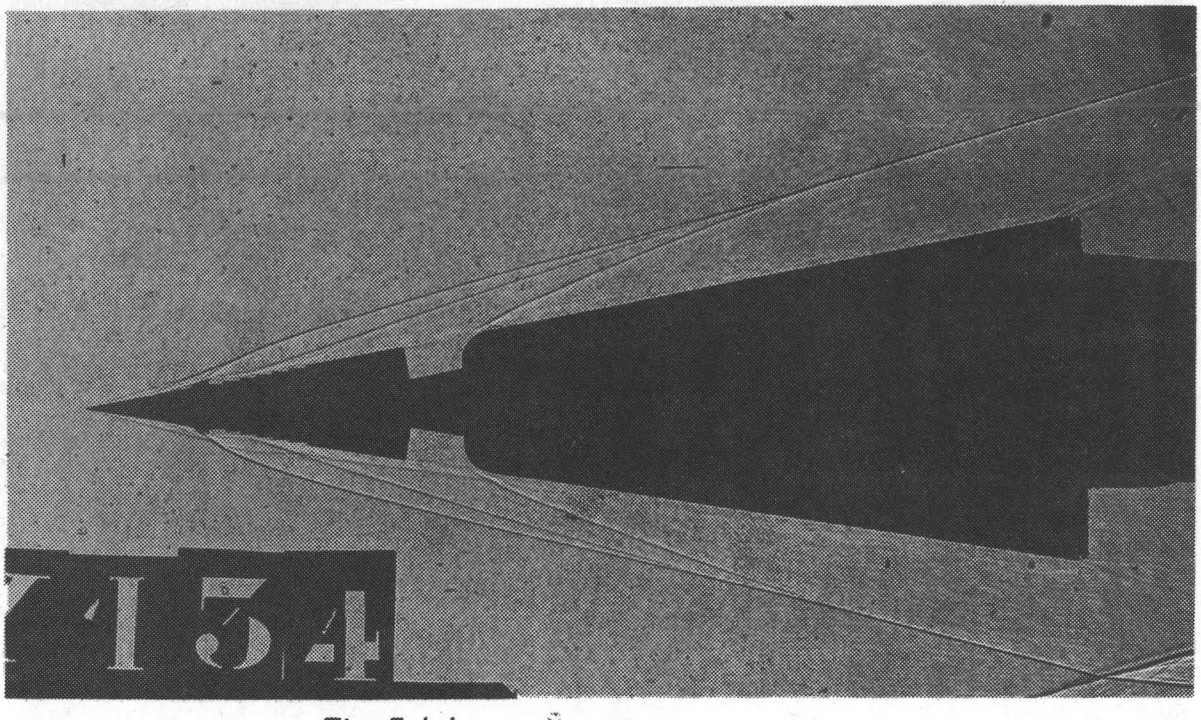

Fig. 5 (c) C_q = .172

SHADOW GRAPHS FOR AIR INJECTION

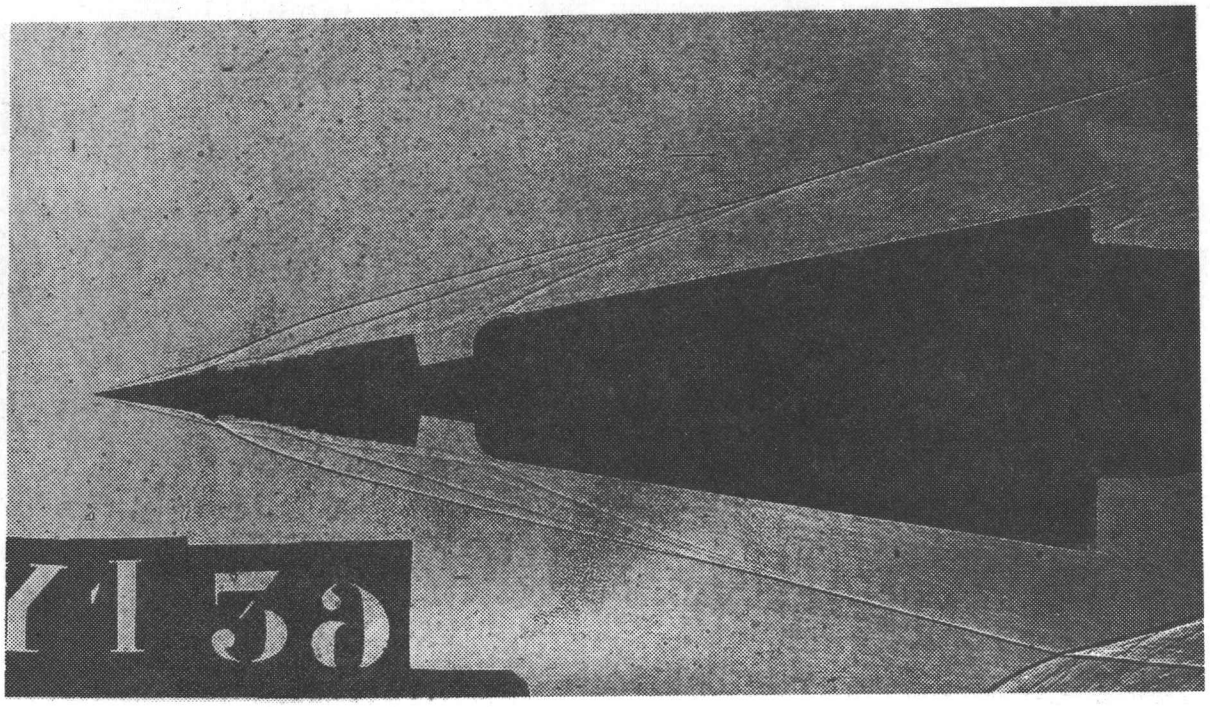

Fig. 5 (d) C_q = .265

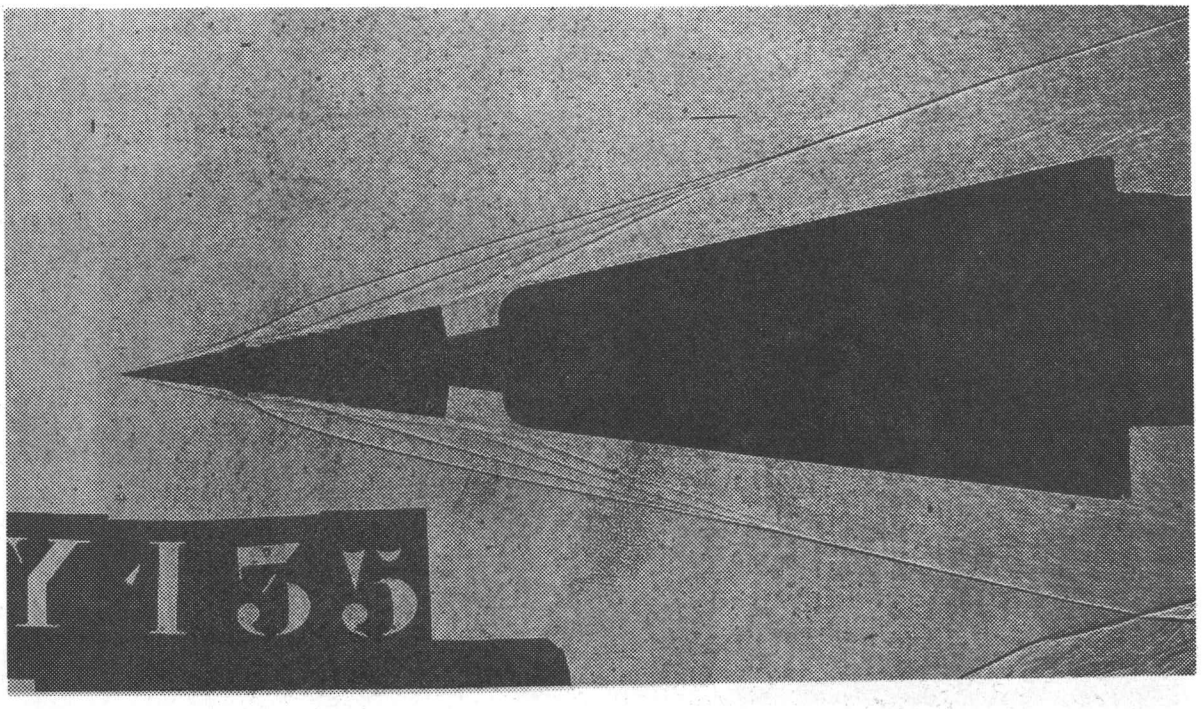

Fig. 5 (e) C_q = .367

SHADOWGRAPHS FOR AIR INJECTION

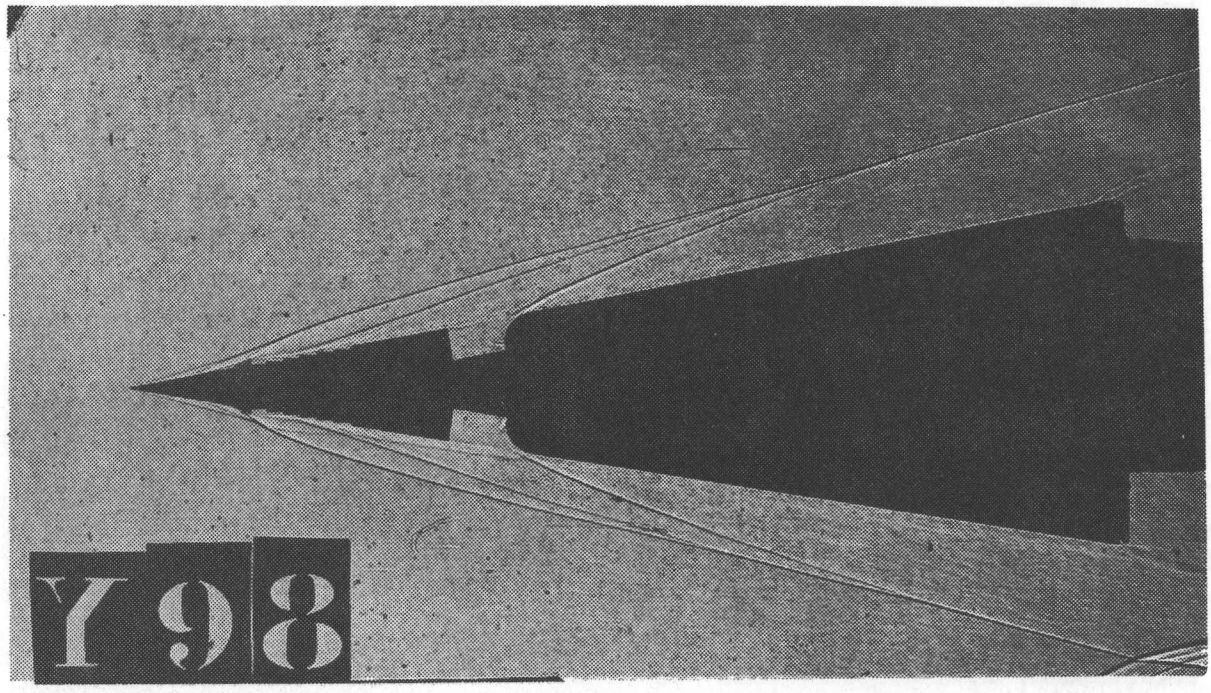

Fig.5 (f). C_q = .042

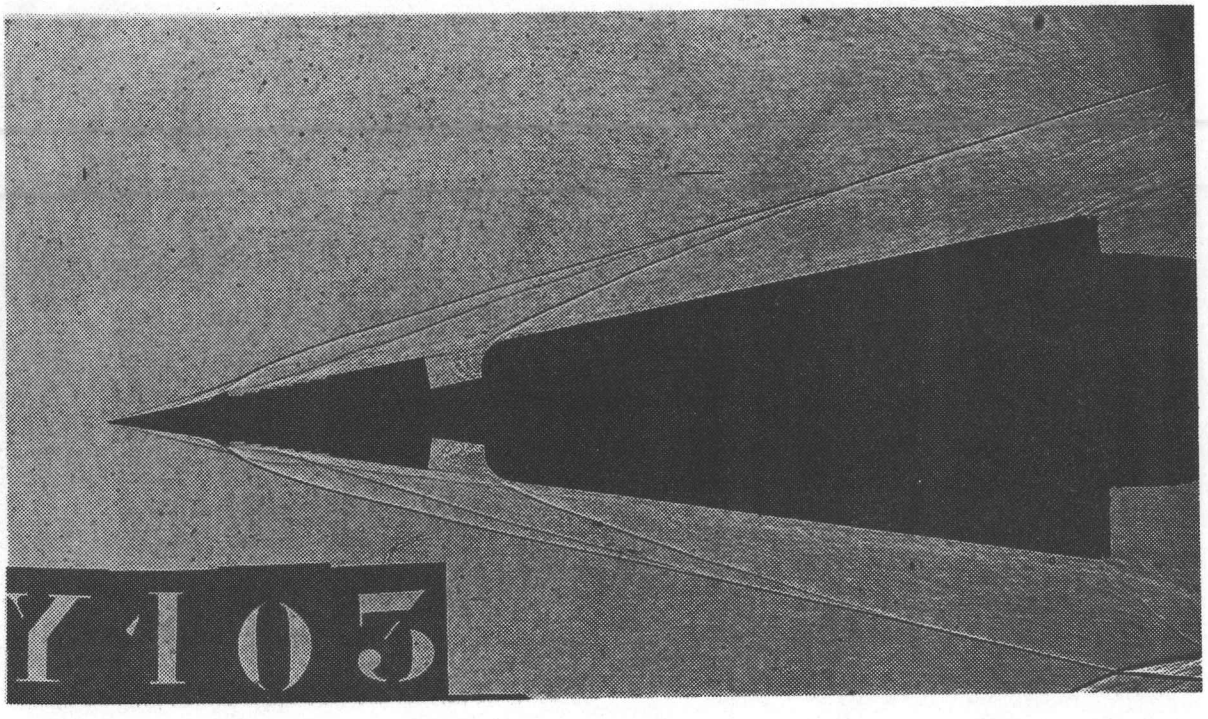

Fig.5 (g) C_q = .181

SHADOWGRAPHS FOR FREON INJECTION

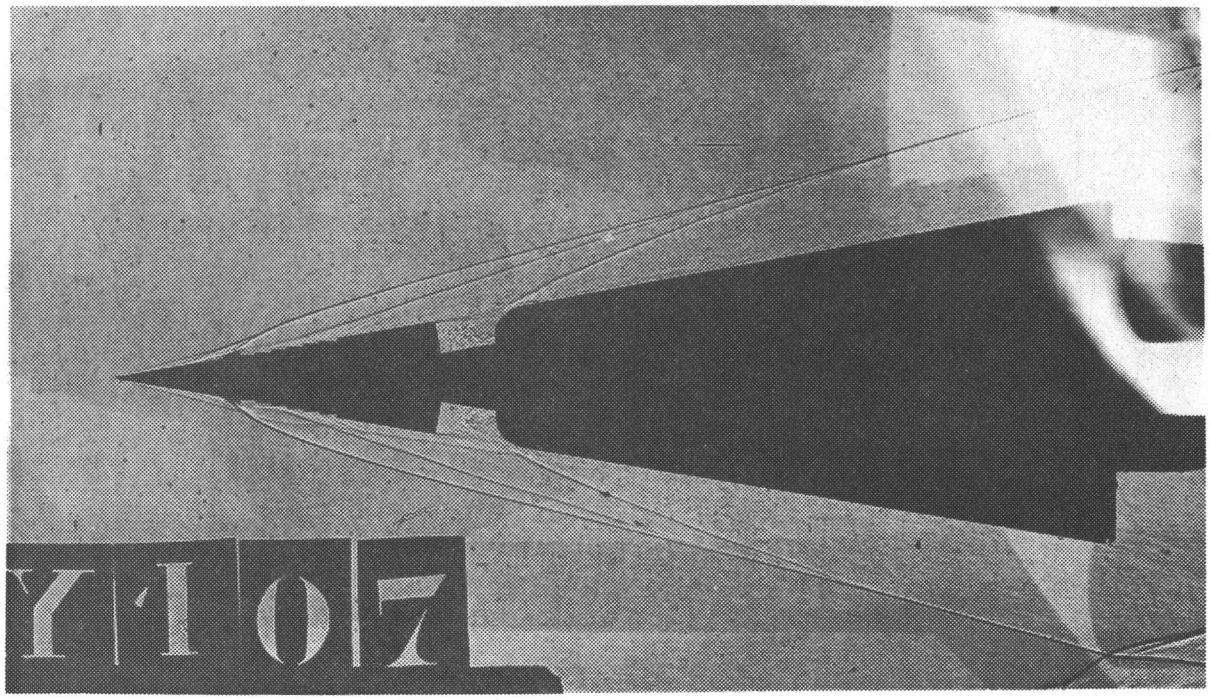

Fig.5 (h). C_q = .248

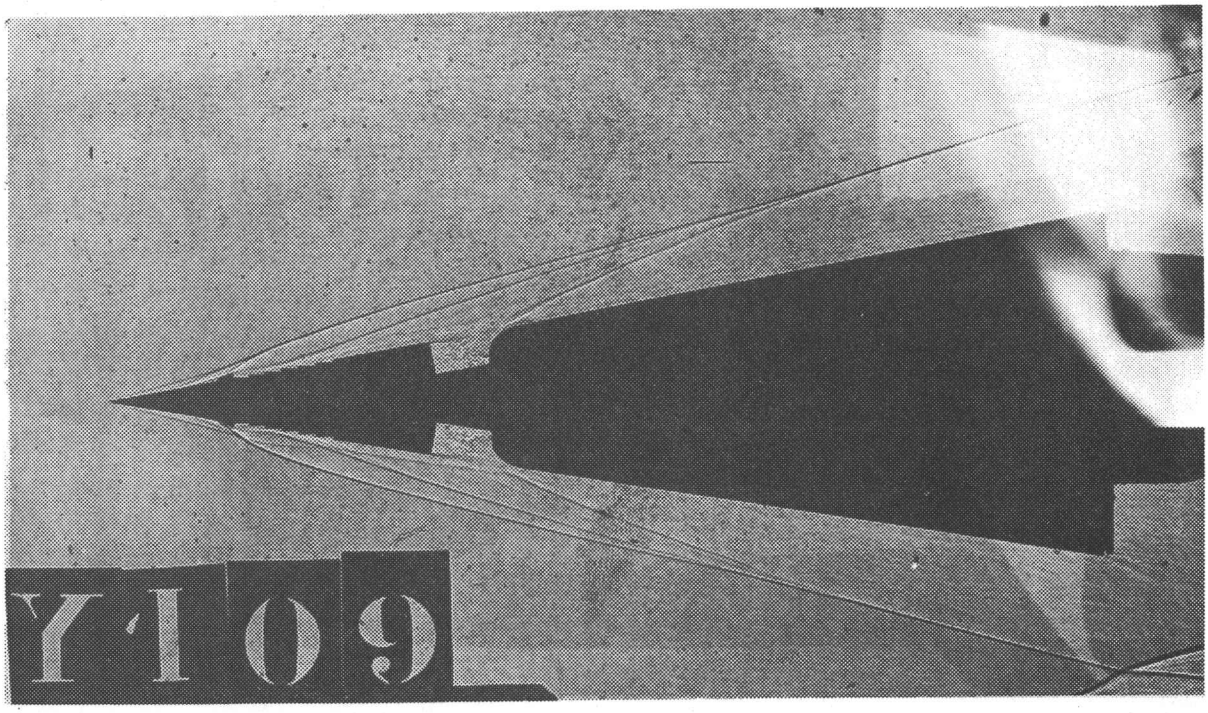

Fig.5 (i). C_q = .385

SHADOWGRAPHS FOR FREON INJECTION

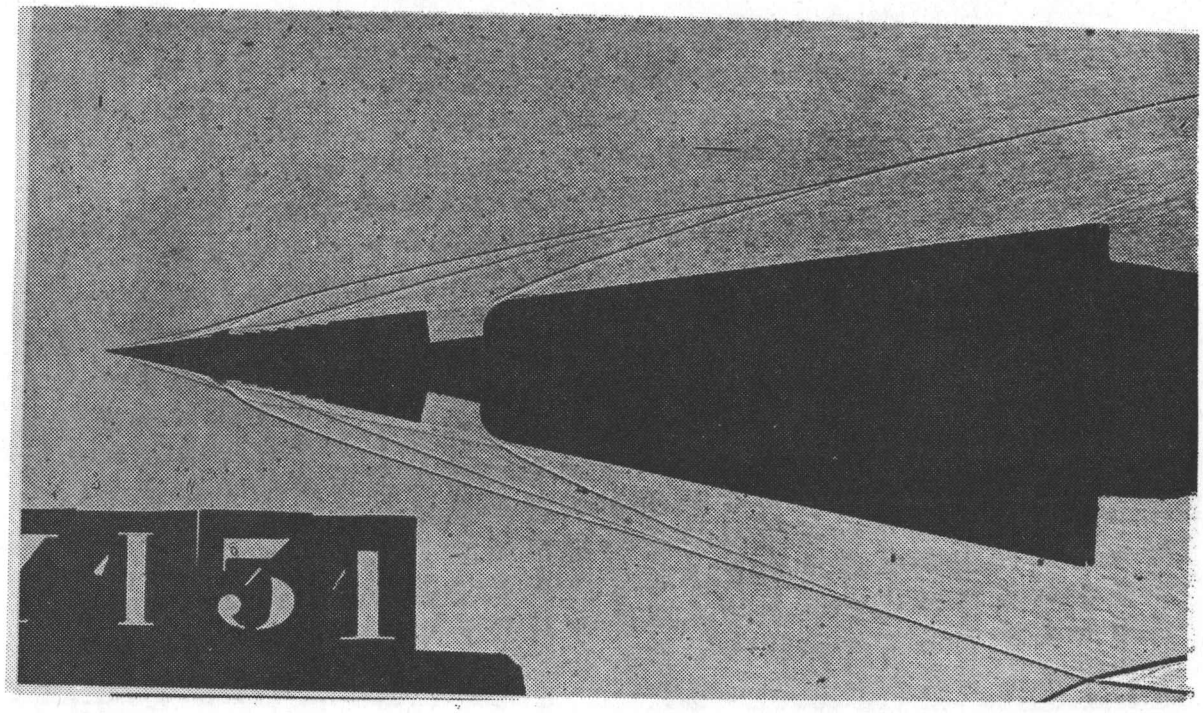

Fig.5 (j). C_q = .018

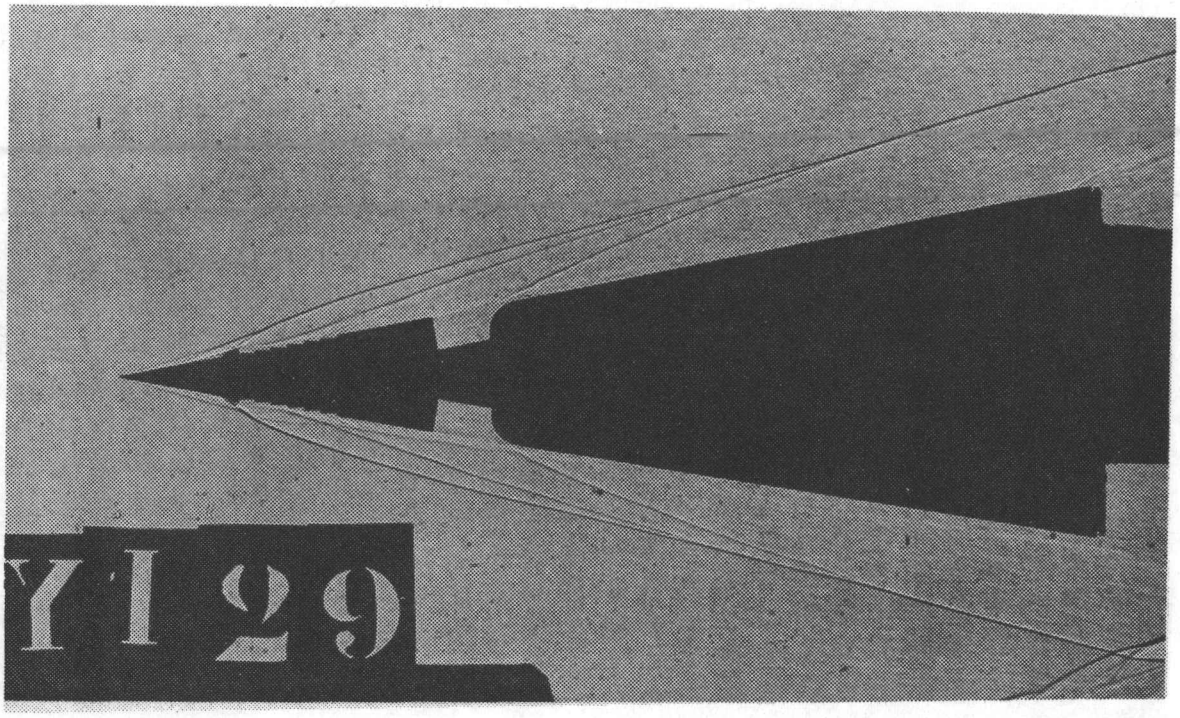

Fig.5 (k). C_q = .053

SHADOWGRAPHS FOR HELIUM INJECTION

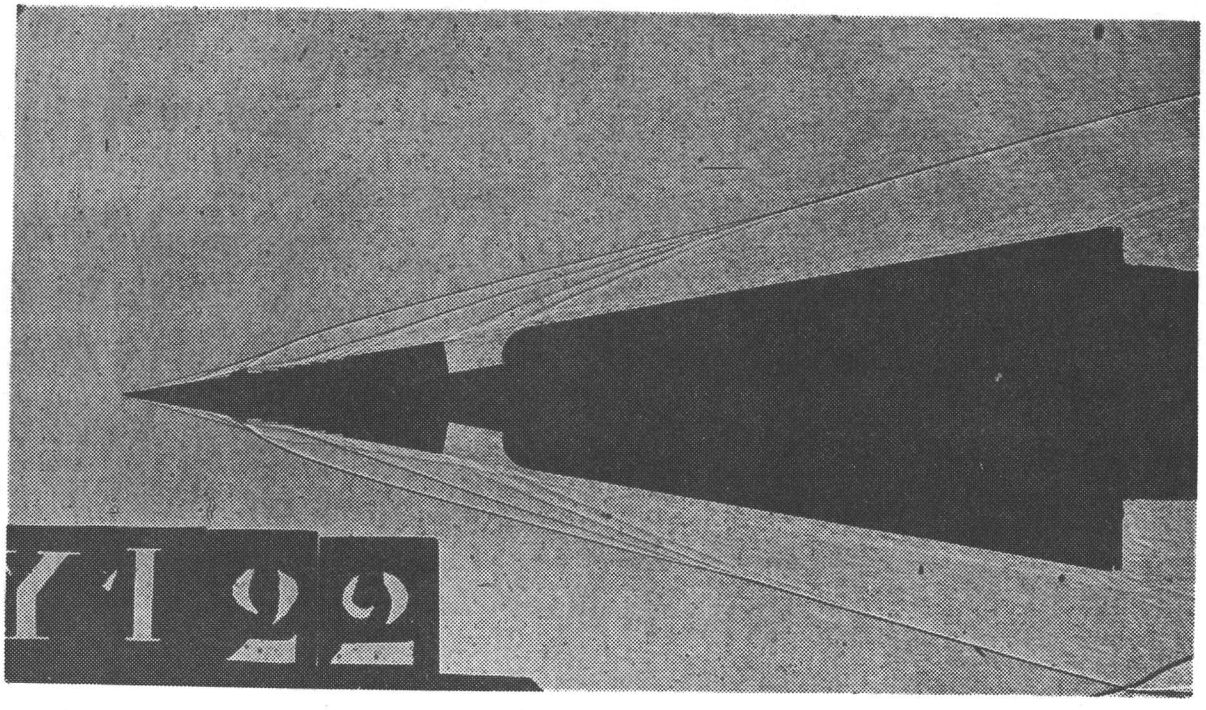

Fig. 5 (L). C_q = .131

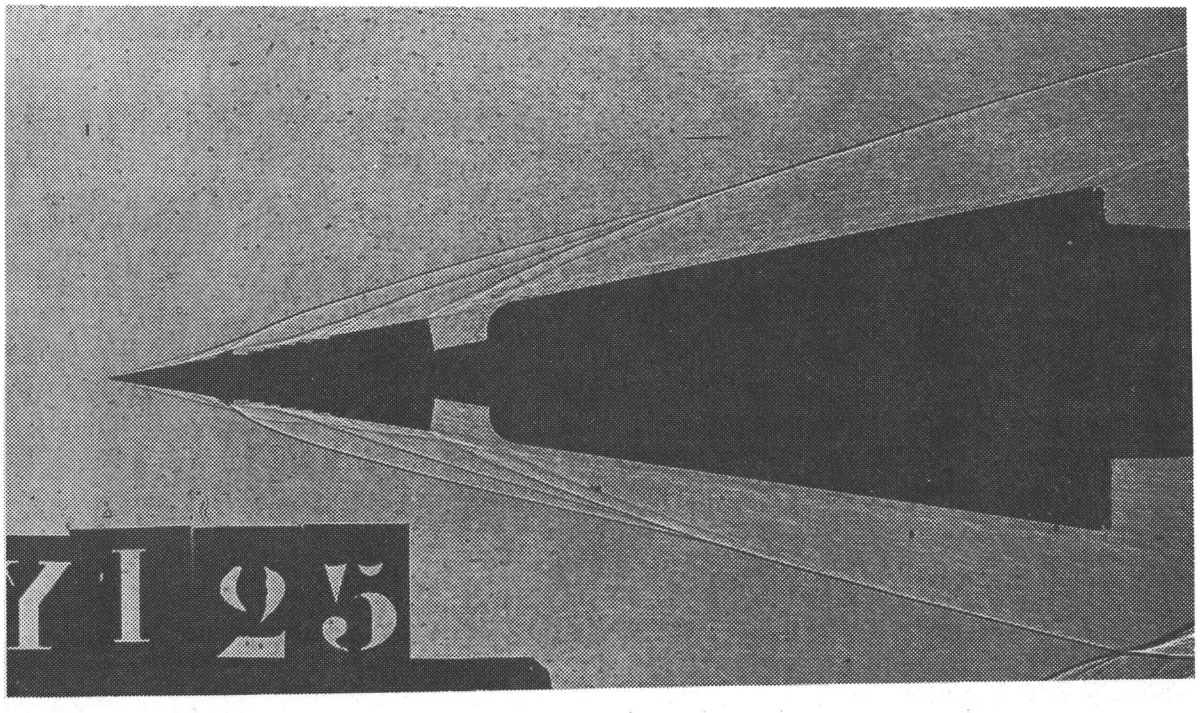

Fig. 5 (m). C_q = .213

SHADOWGRAPHS FOR HELIUM INJECTION

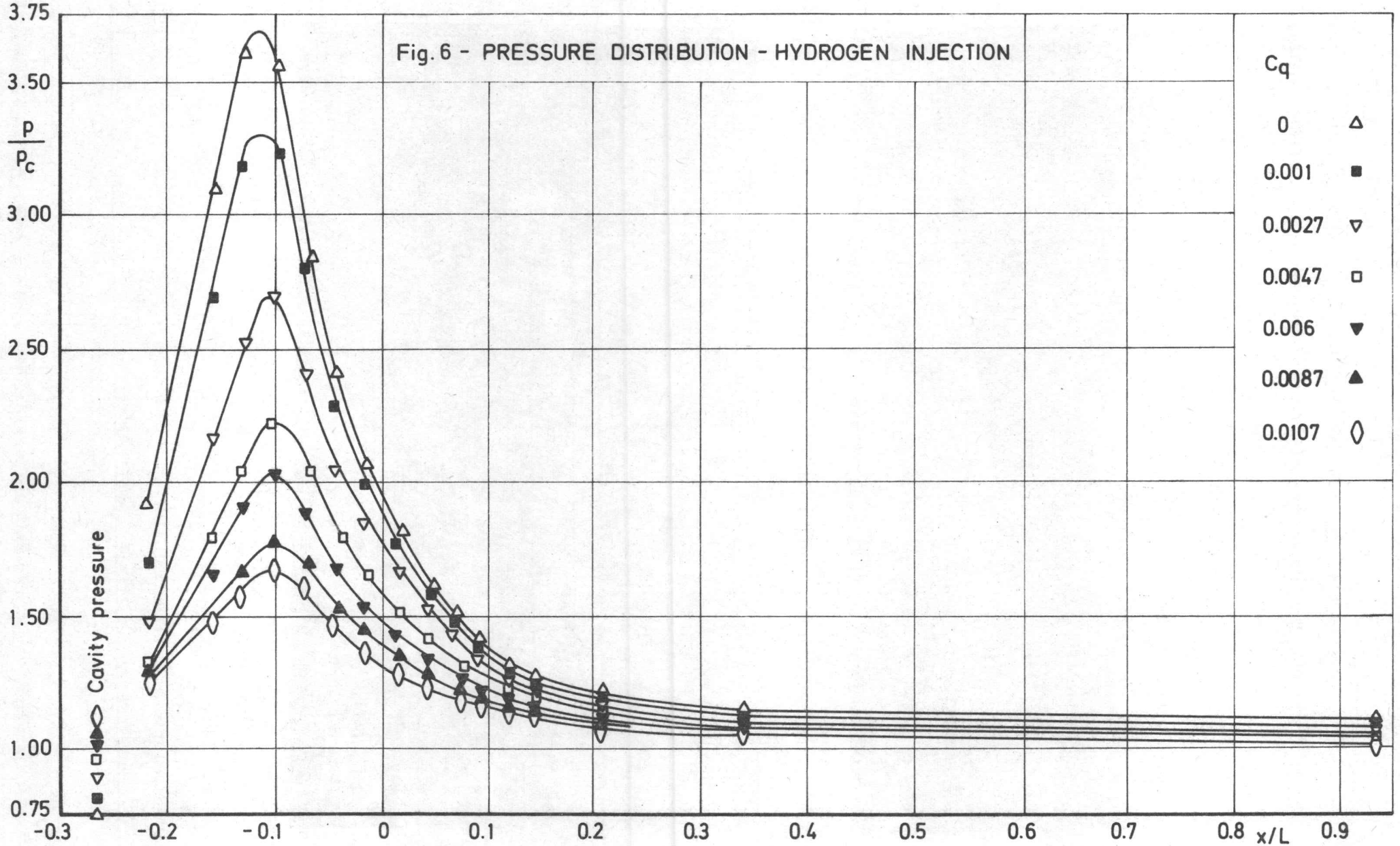
Fig. 6 - PRESSURE DISTRIBUTION - HYDROGEN INJECTION
P/Pc
3.75
3.50
3.00
2.50
2.00
1.50
1.00
0.75
-0.3
-0.2
-0.1
0
0.1
0.2
0.3
0.4
0.5
0.6
0.7
0.8
0.9
x/L
Cavity pressure
Cq
0
0.001
0.0027
0.0047
0.006
0.0087
0.0107

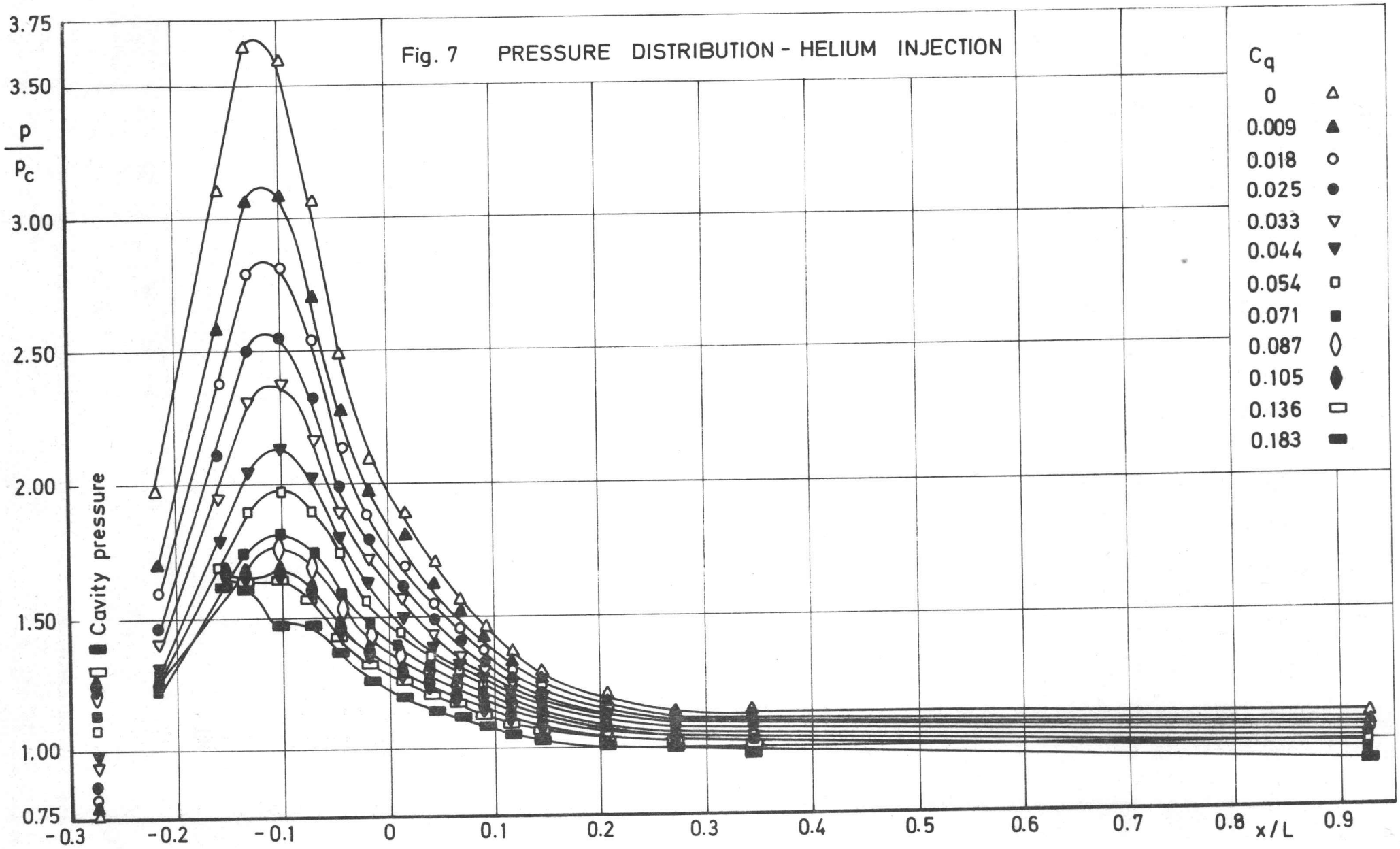
Fig. 7 PRESSURE DISTRIBUTION - HELIUM INJECTION
3.75
3.50
P/Pc
3.00
2.50
2.00
1.50
1.00
0.75
-0.3
-0.2
-0.1
0
0.1
0.2
0.3
0.4
0.5
0.6
0.7
0.8
0.9
x/L
Cavity pressure
Cq
0
0.009
0.018
0.025
0.033
0.044
0.054
0.071
0.087
0.105
0.136
0.183

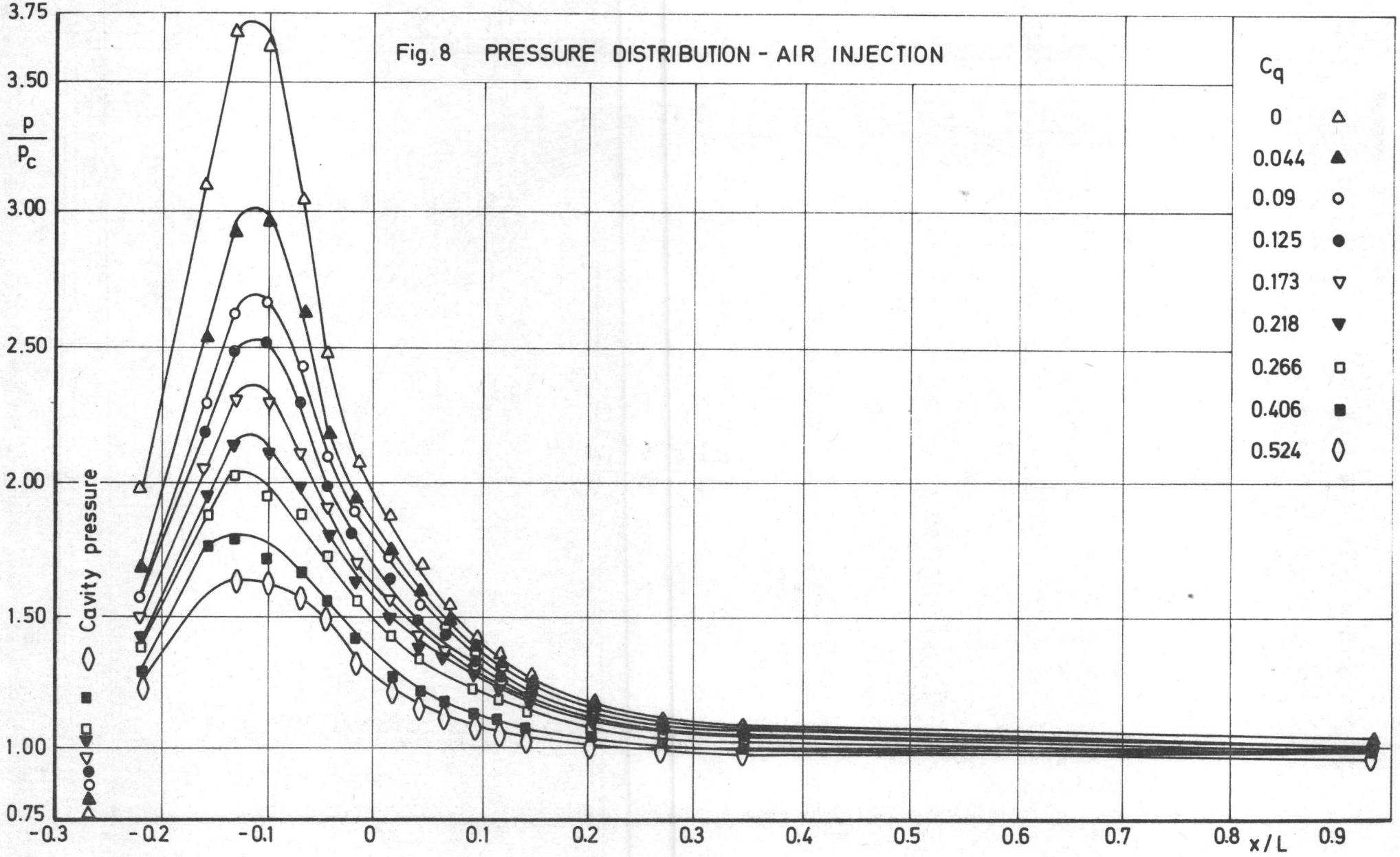
Fig. 8 PRESSURE DISTRIBUTION - AIR INJECTION
$\frac{p}{p_c}$
3.75
3.50
3.00
2.50
2.00
1.50
1.00
0.75
-0.3
-0.2
-0.1
0
0.1
0.2
0.3
0.4
0.5
0.6
0.7
0.8
0.9
x/L
Cavity pressure
C_q
0
0.044
0.09
0.125
0.173
0.218
0.266
0.406
0.524

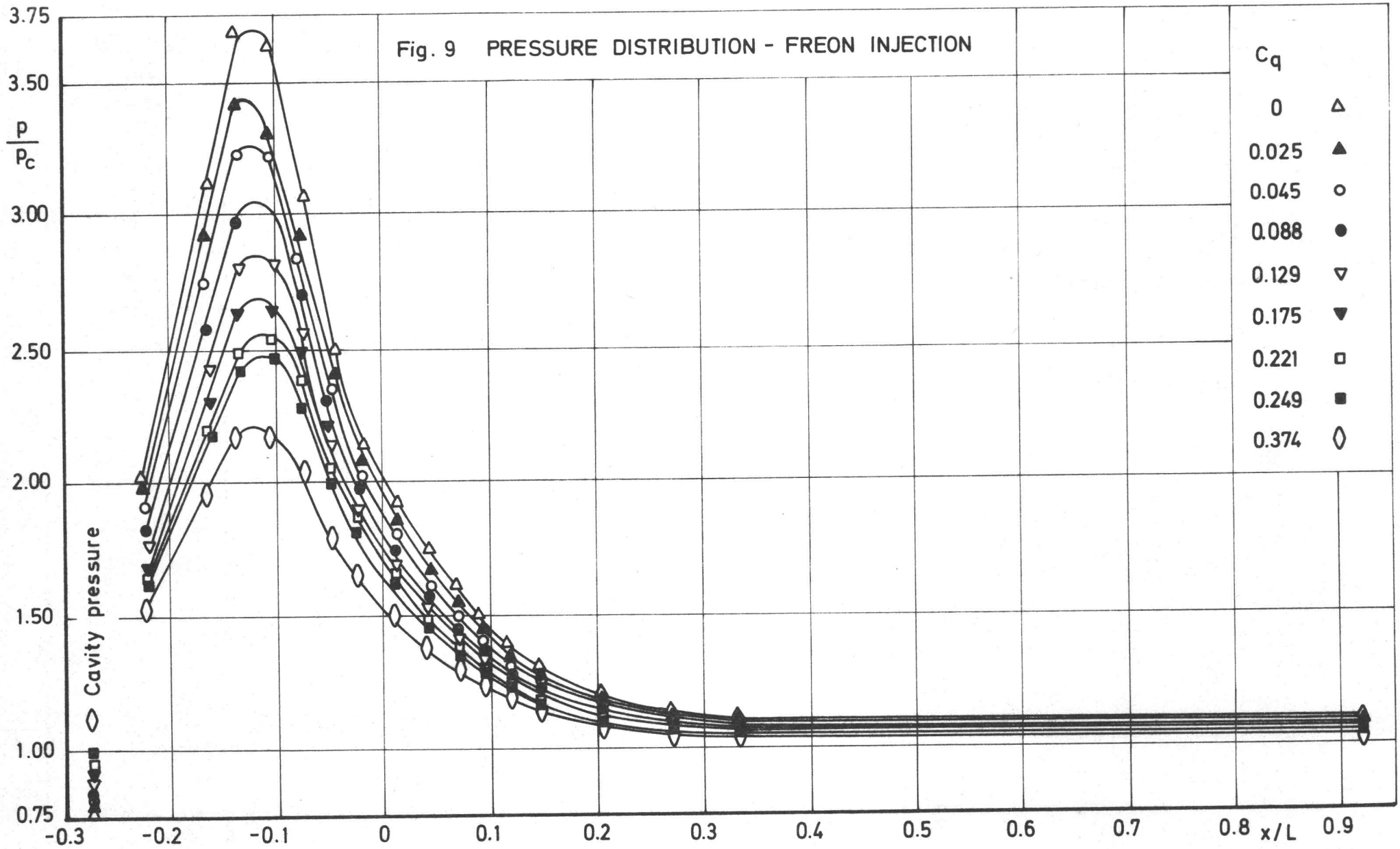
Fig. 9 PRESSURE DISTRIBUTION - FREON INJECTION
$\frac{P}{P_c}$
3.75
3.50
3.00
2.50
2.00
1.50
1.00
0.75
-0.3
-0.2
-0.1
0
0.1
0.2
0.3
0.4
0.5
0.6
0.7
0.8
0.9
x/L
◇ Cavity pressure
C_q
0
0.025
0.045
0.088
0.129
0.175
0.221
0.249
0.374

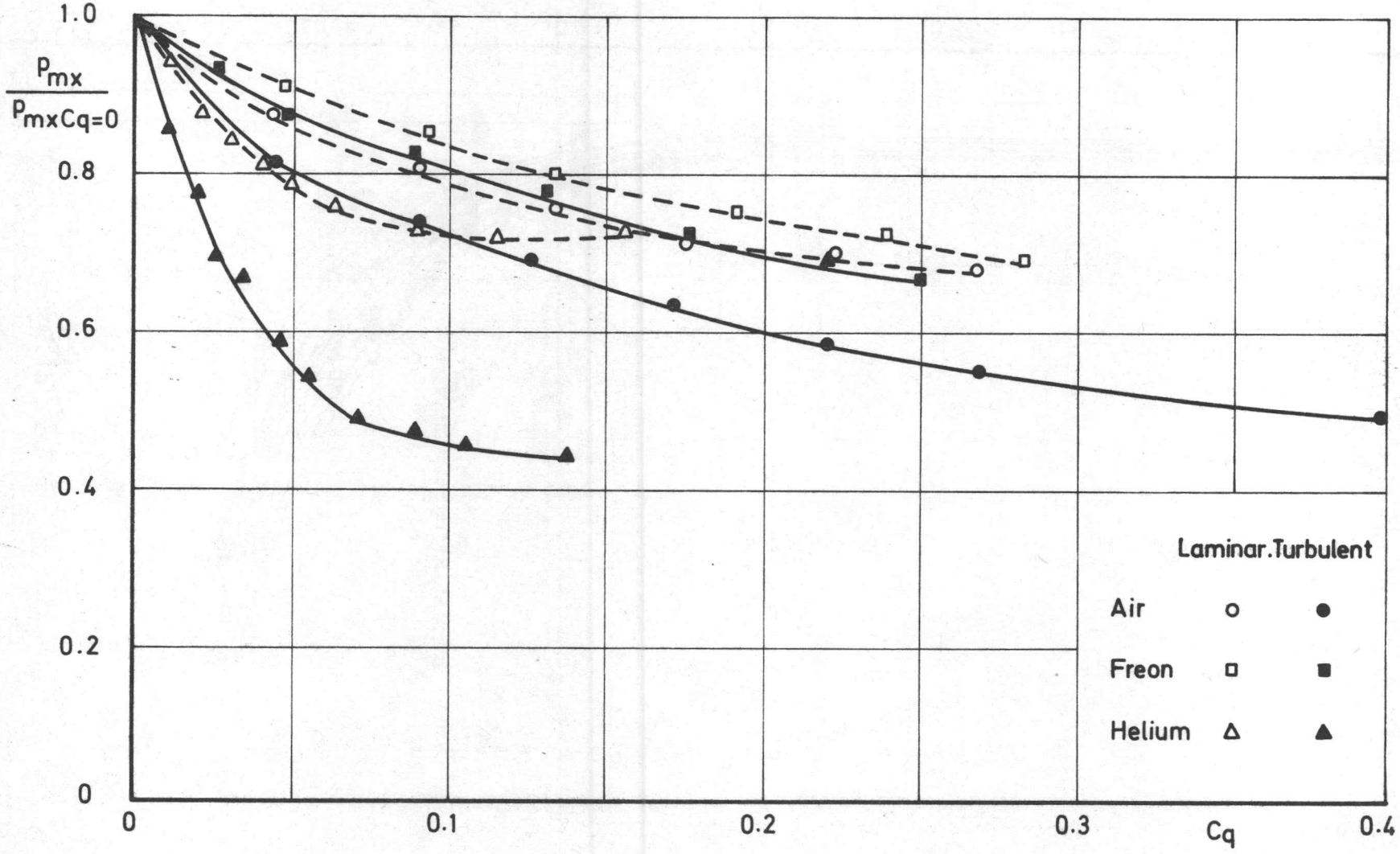

Fig. 10 - EFFECTIVENESS OF GAS INJECTION ON PRESSURE PEAK.

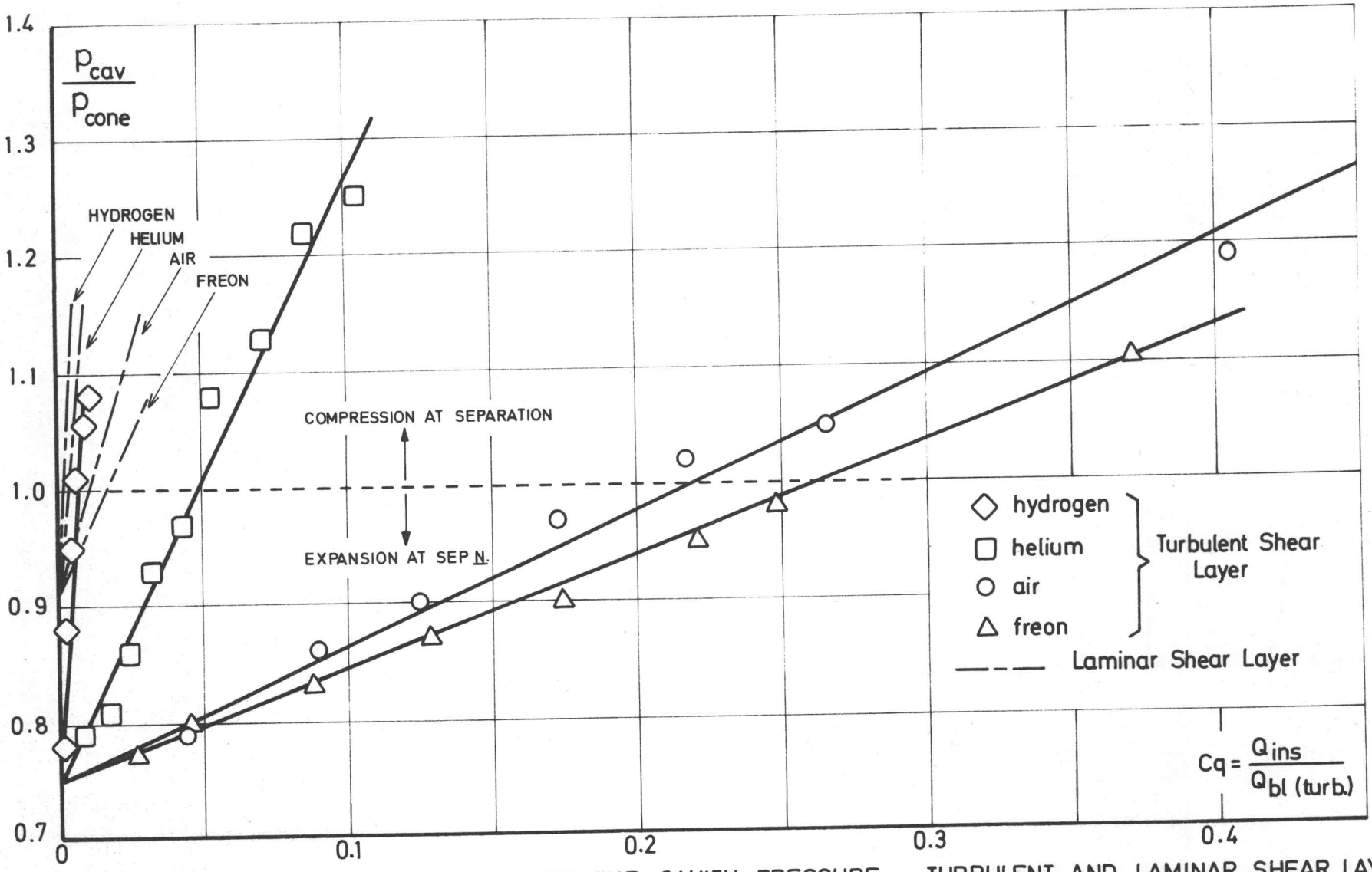

Fig.11 - EFFECT OF INJECTANT MASS FLOW ON THE CAVITY PRESSURE - TURBULENT AND LAMINAR SHEAR LAYER.

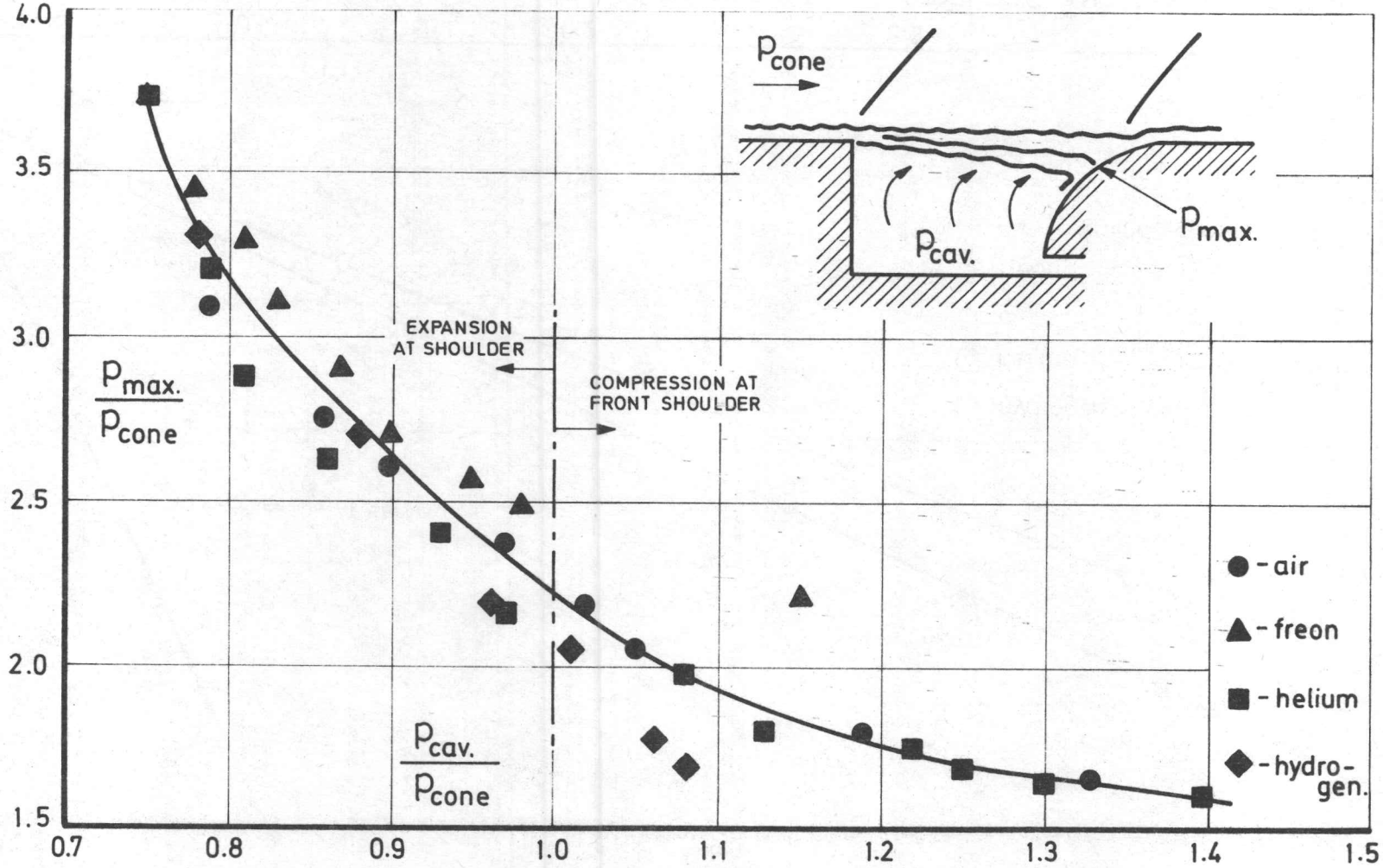

Fig.12 - CORRELATION OF PEAK PRESSURES AT REATTACHMENT. TURBULENT BOUNDARY LAYER.

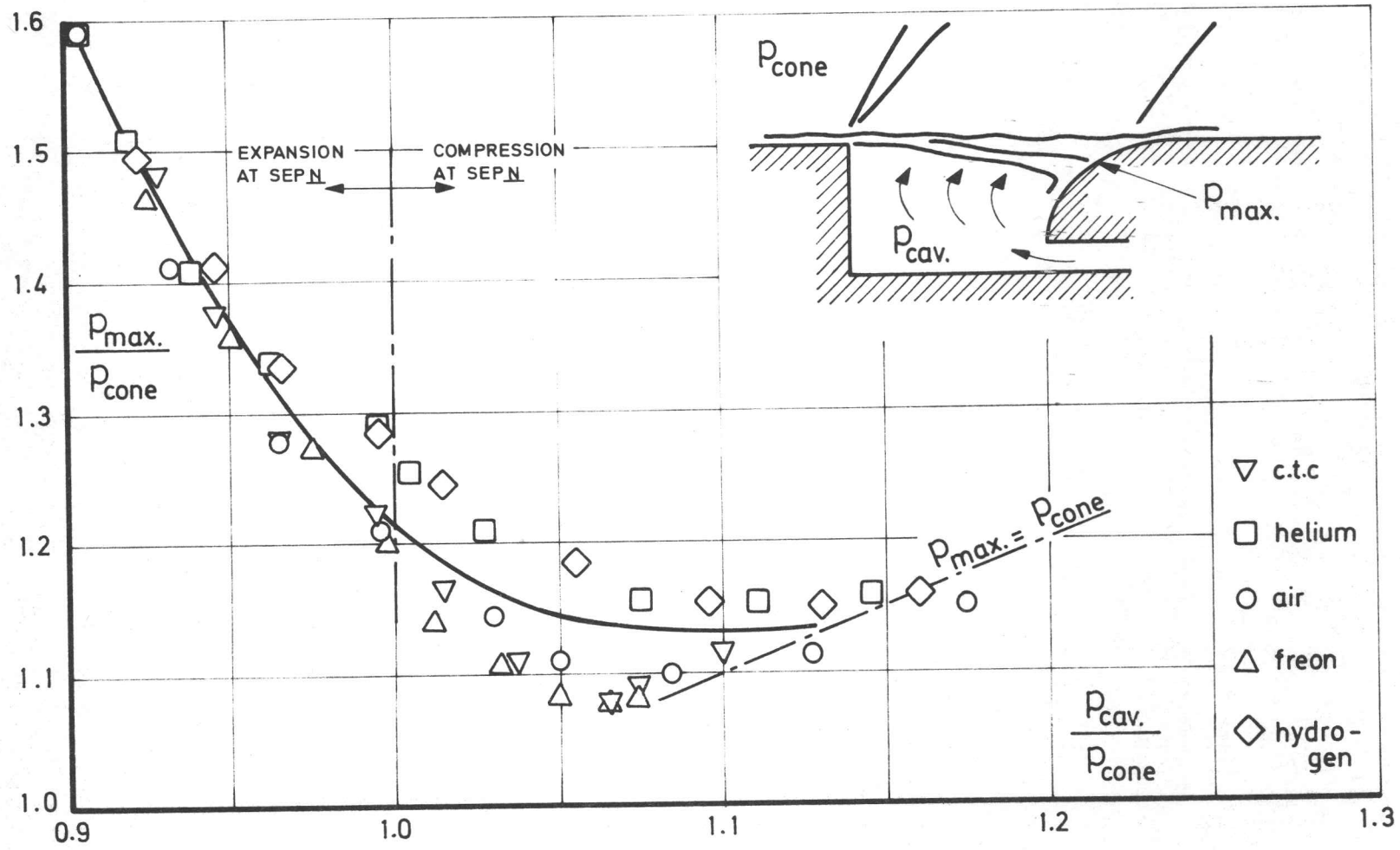

Fig. 13 - CORRELATIONS OF PEAK PRESSURES AT REATTACHMENT. LAMINAR FLOW.

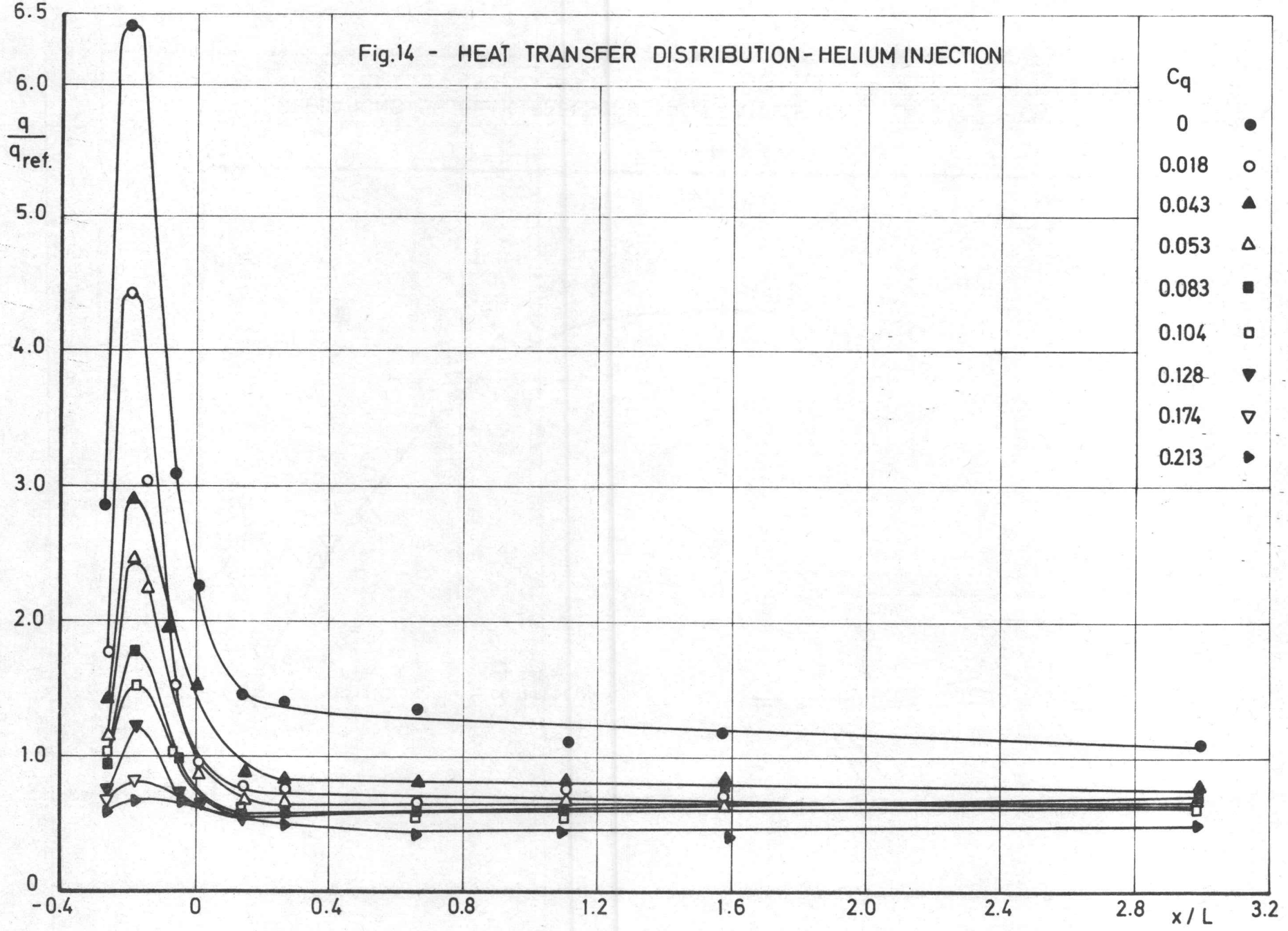
Fig.14 - HEAT TRANSFER DISTRIBUTION - HELIUM INJECTION
$\frac{q}{q_{ref.}}$
6.5
6.0
5.0
4.0
3.0
2.0
1.0
0
-0.4
0
0.4
0.8
1.2
1.6
2.0
2.4
2.8
3.2
x / L
C_q
0
0.018
0.043
0.053
0.083
0.104
0.128
0.174
0.213

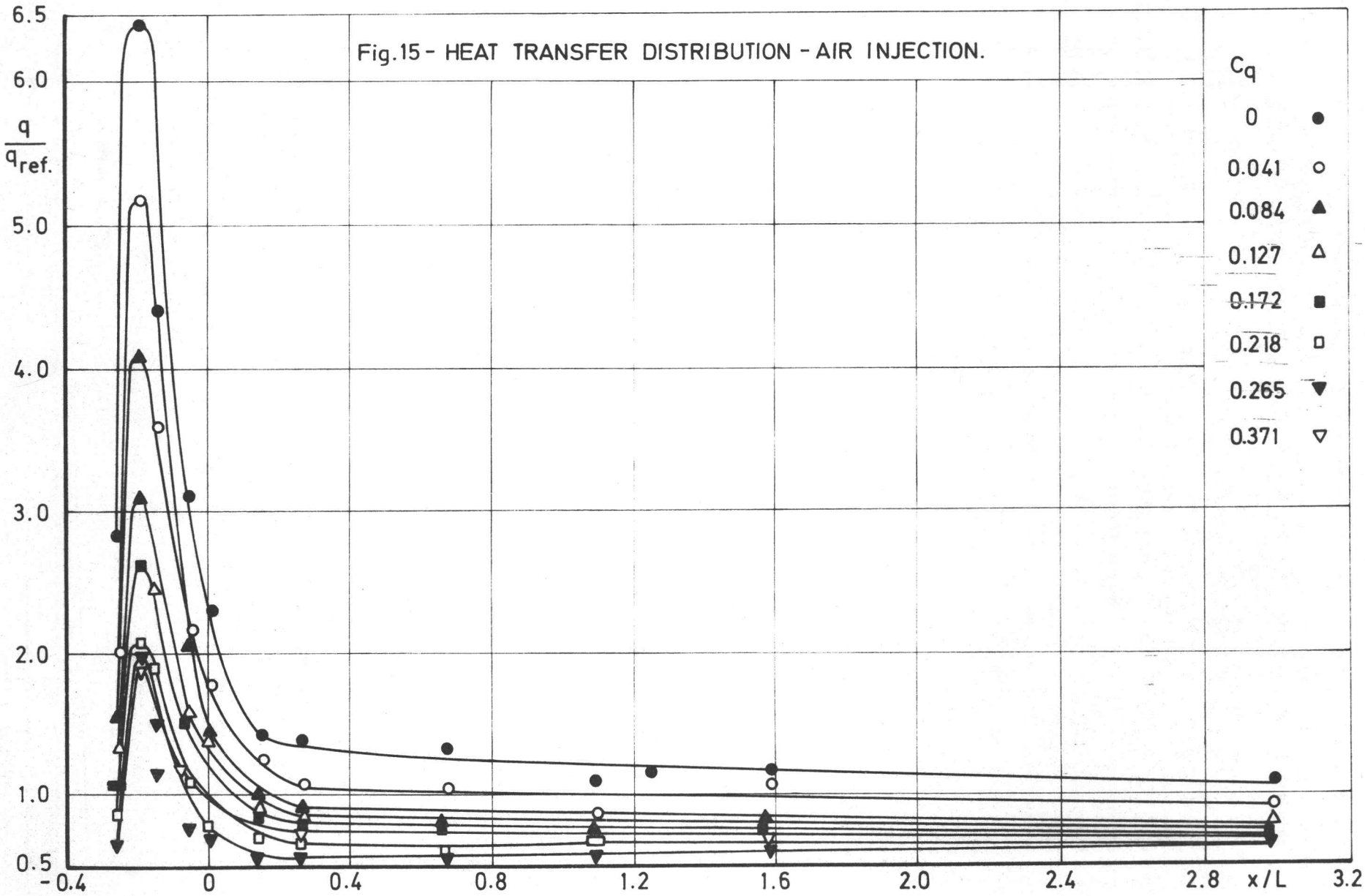
Fig.15 - HEAT TRANSFER DISTRIBUTION - AIR INJECTION.
$\frac{q}{q_{ref.}}$
6.5
6.0
5.0
4.0
3.0
2.0
1.0
0.5
-0.4
0
0.4
0.8
1.2
1.6
2.0
2.4
2.8
x/L
3.2
C_q
0
0.041
0.084
0.127
0.172
0.218
0.265
0.371

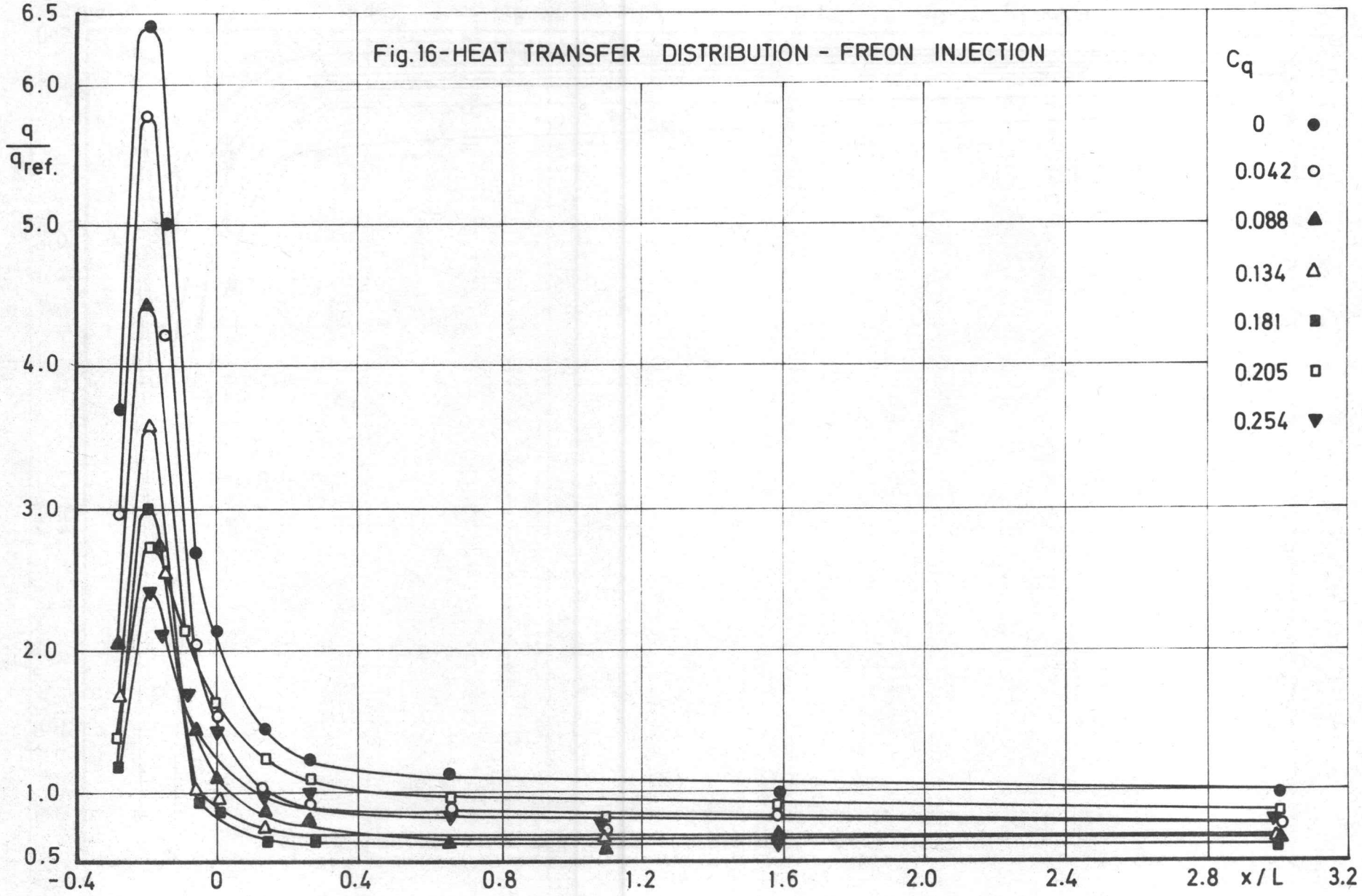
Fig.16-HEAT TRANSFER DISTRIBUTION - FREON INJECTION
$\frac{q}{q_{ref.}}$
6.5
6.0
5.0
4.0
3.0
2.0
1.0
0.5
-0.4
0
0.4
0.8
1.2
1.6
2.0
2.4
2.8
x / L
3.2
C_q
0
0.042
0.088
0.134
0.181
0.205
0.254

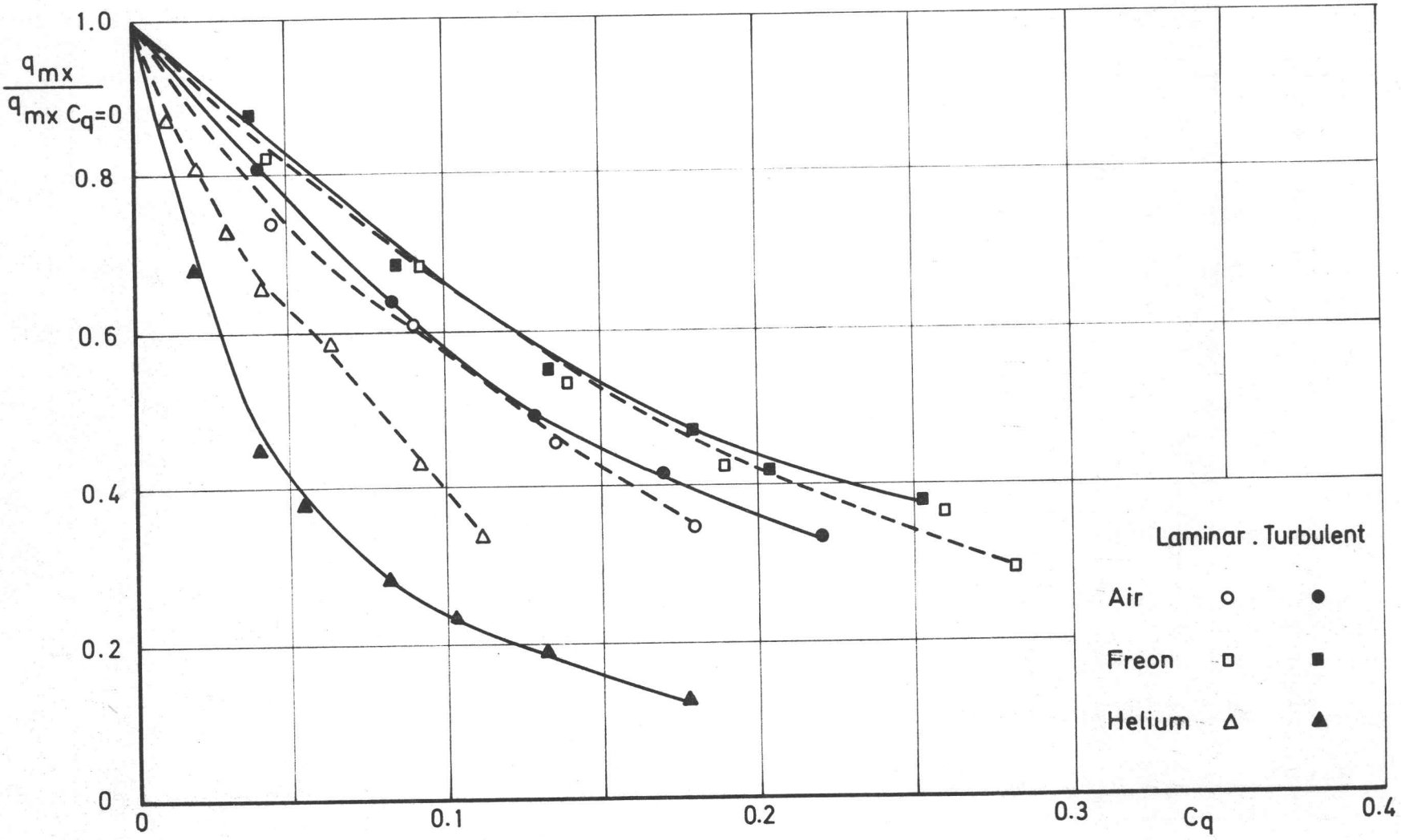

Fig.17 - EFFECTIVENESS OF GAS INJECTION ON HEAT TRANSFER PEAK.

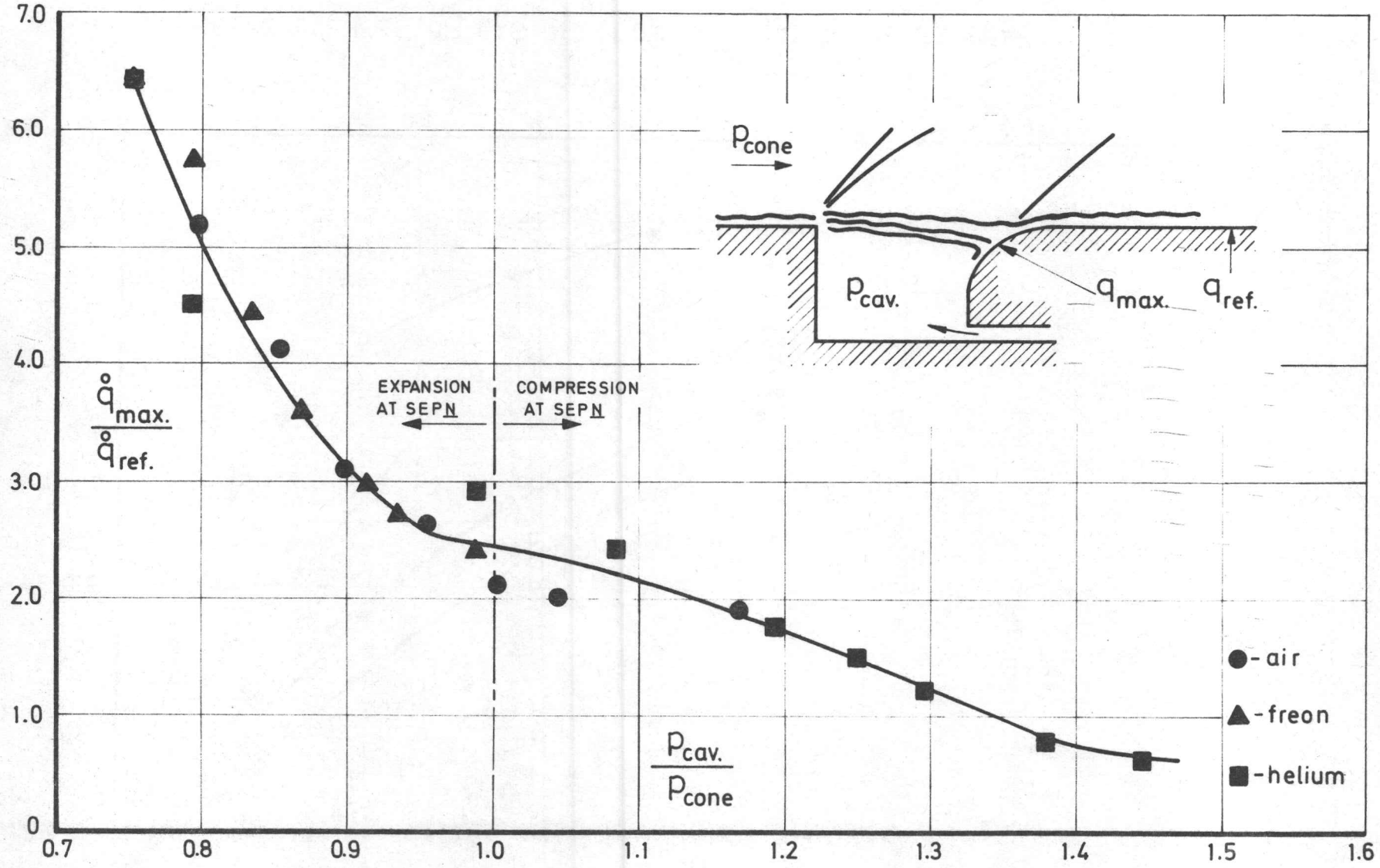

Fig.18 - CORRELATION OF PEAK HEATING AT REATTACHMENT. TURBULENT BOUNDARY LAYER.

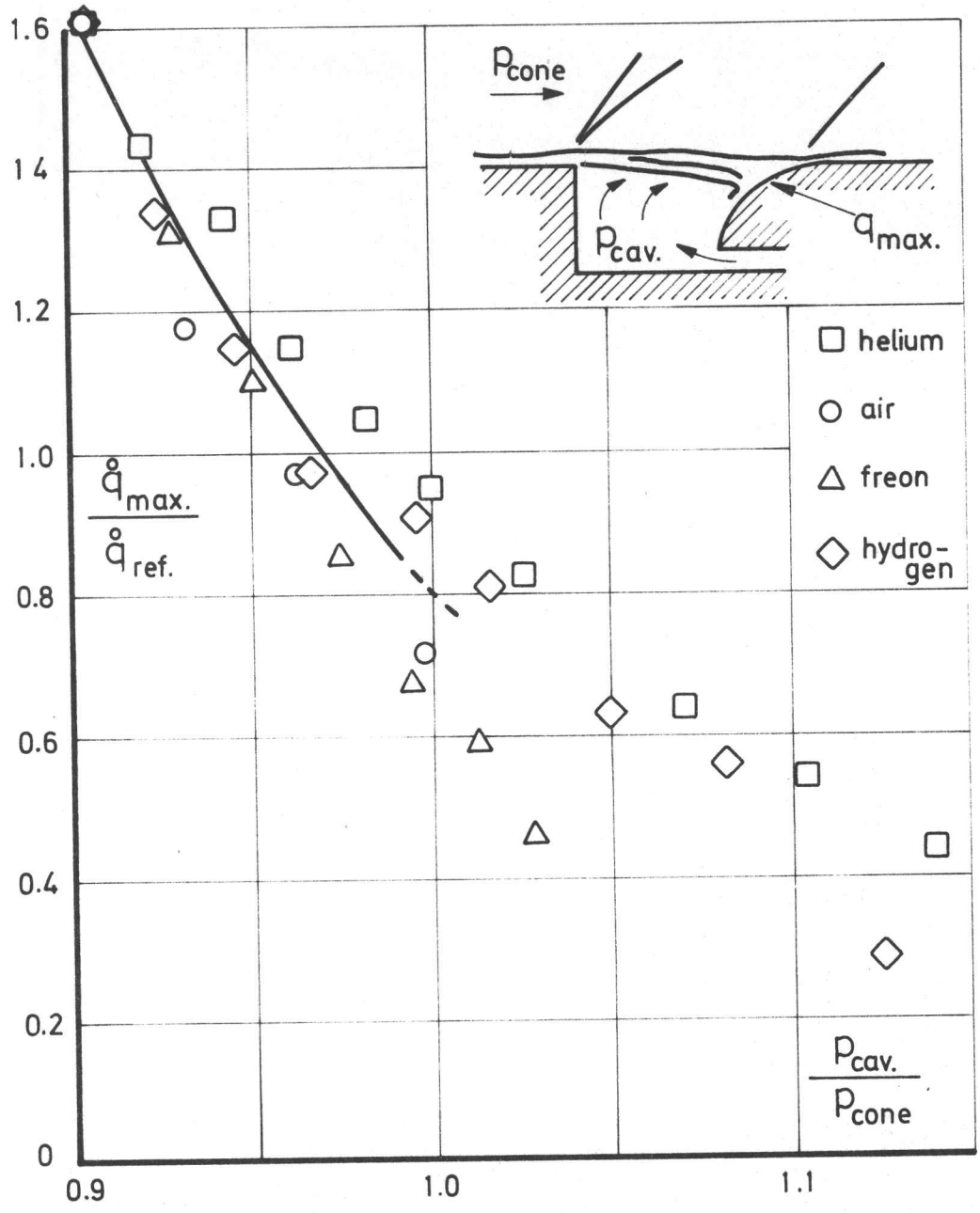

Fig.19. CORRELATIONS OF PEAK HEATING AT REATTACHMENT. LAMINAR FLOW

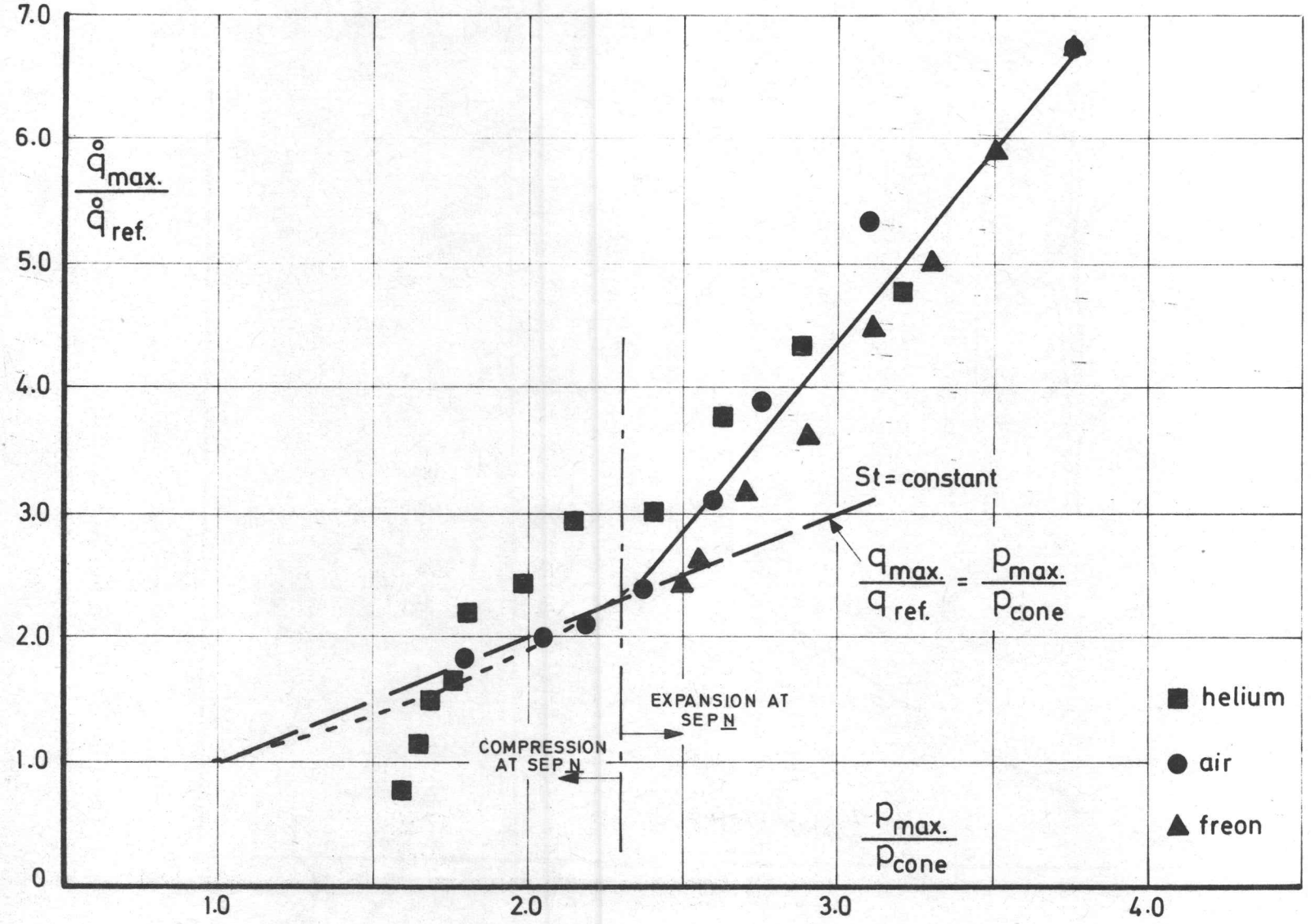

Fig. 20 - CORRELATION OF PEAK HEATING WITH PEAK PRESSURE. TURBULENT BOUNDARY LAYER.

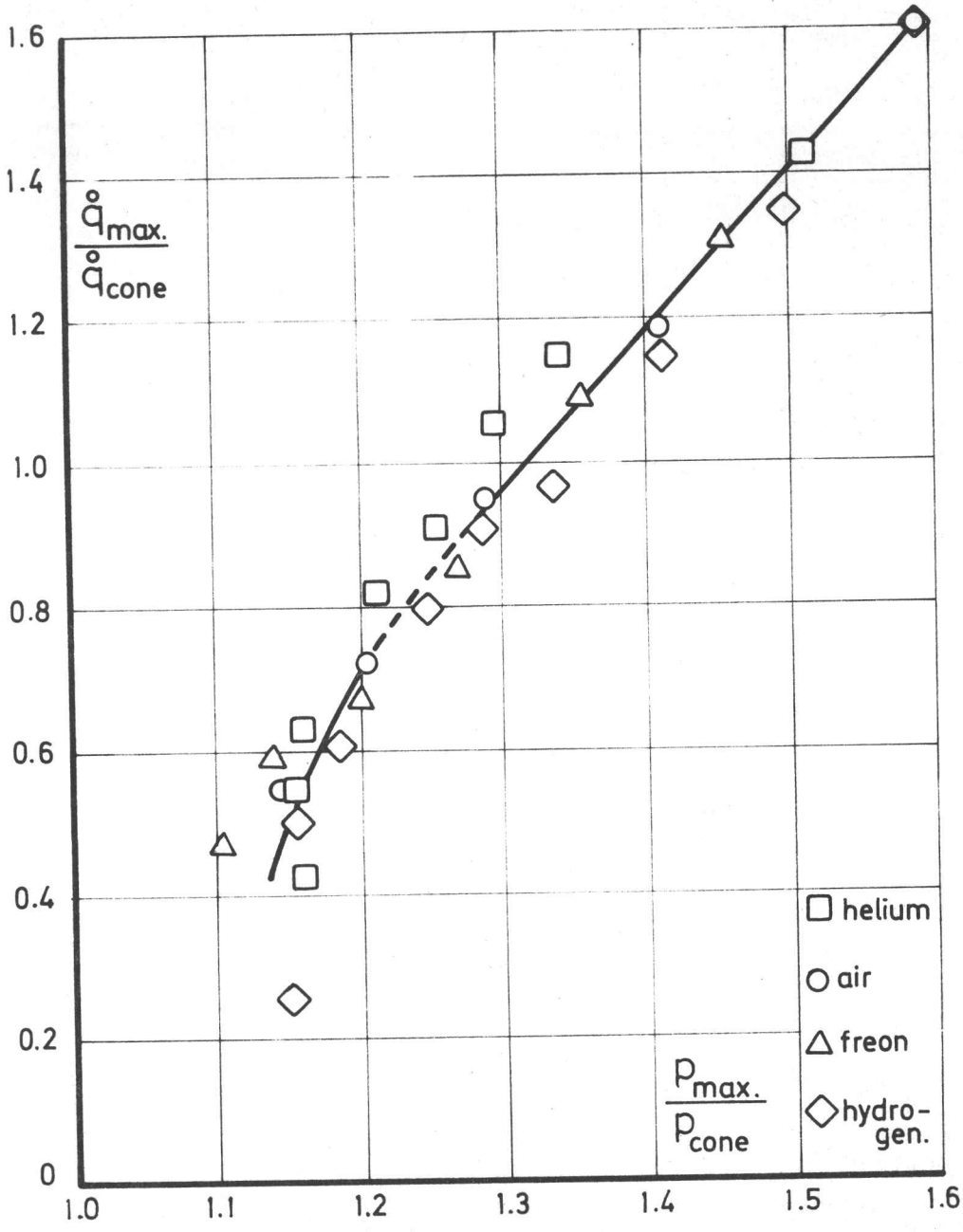

Fig. 21 - CORRELATION OF PEAK HEATING WITH PEAK PRESSURE. LAMINAR BOUNDARY LAYER.

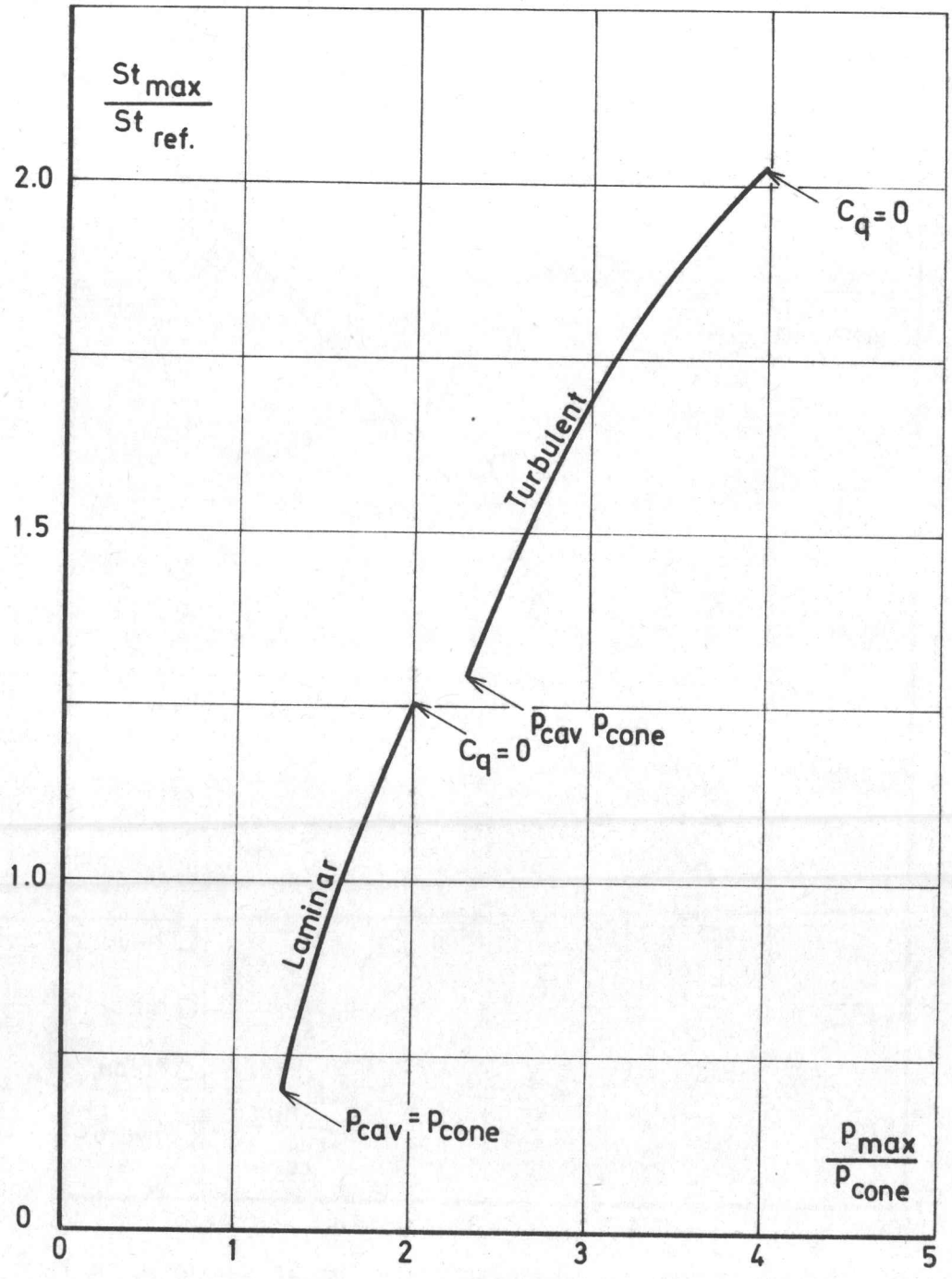

Fig. 22 - REATTACHMENT STANTON NUMBERS.

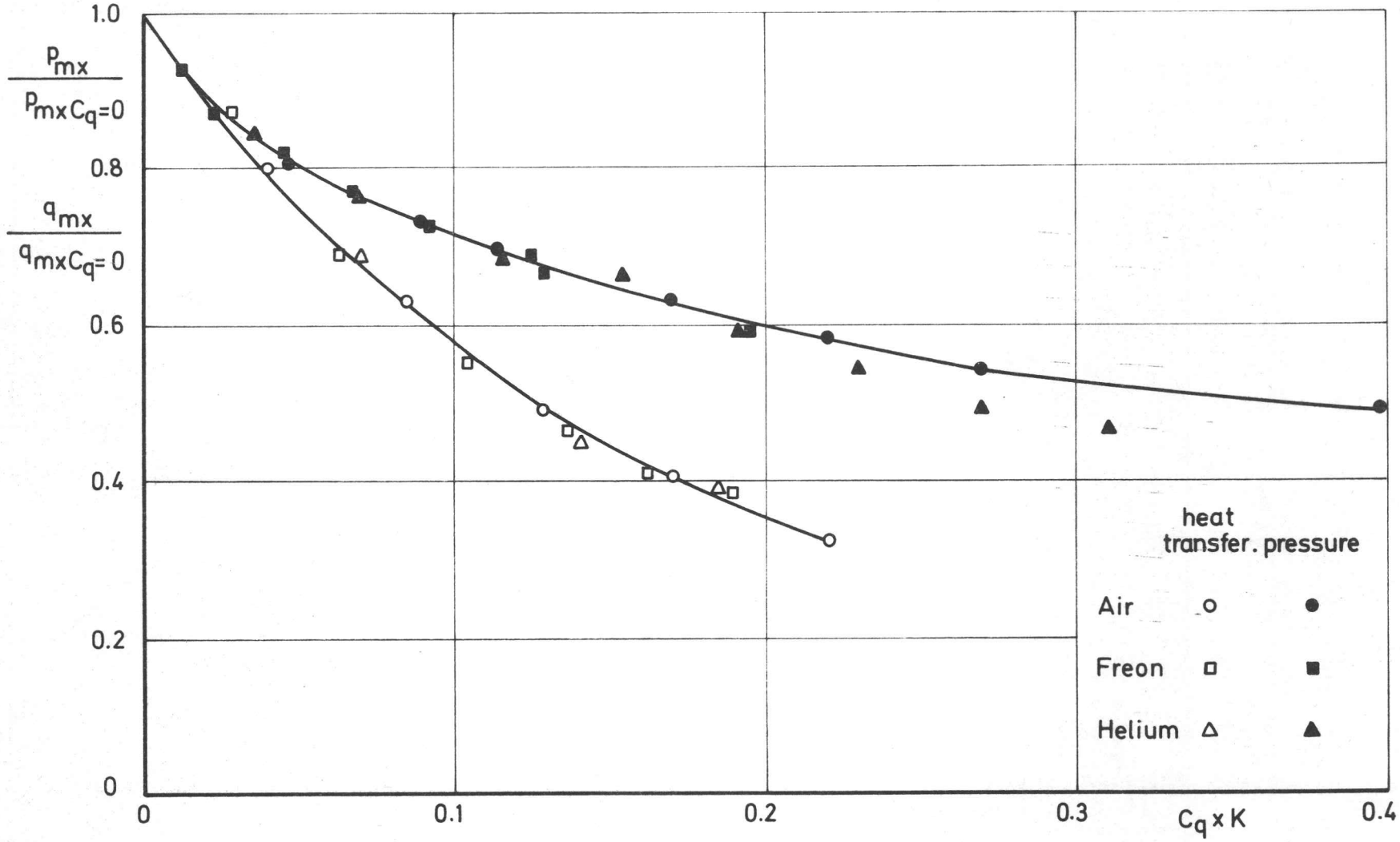

Fig. 23 - CORRELATION OF PEAK PRESSURE AND HEAT TRANSFER RATIOS.

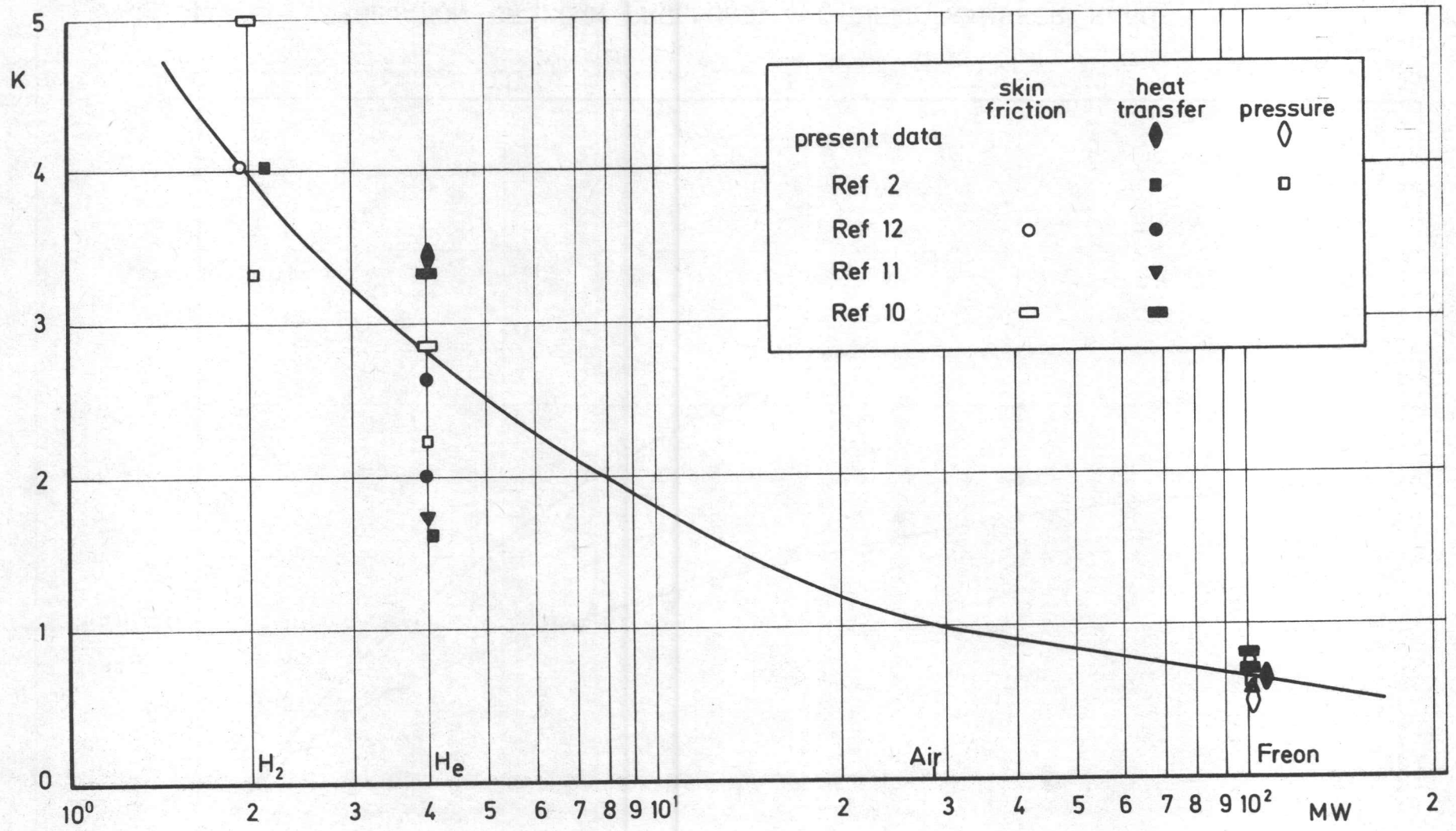

Fig. 24 - CORRELATION FACTOR K VERSUS MOLECULAR WEIGHT.

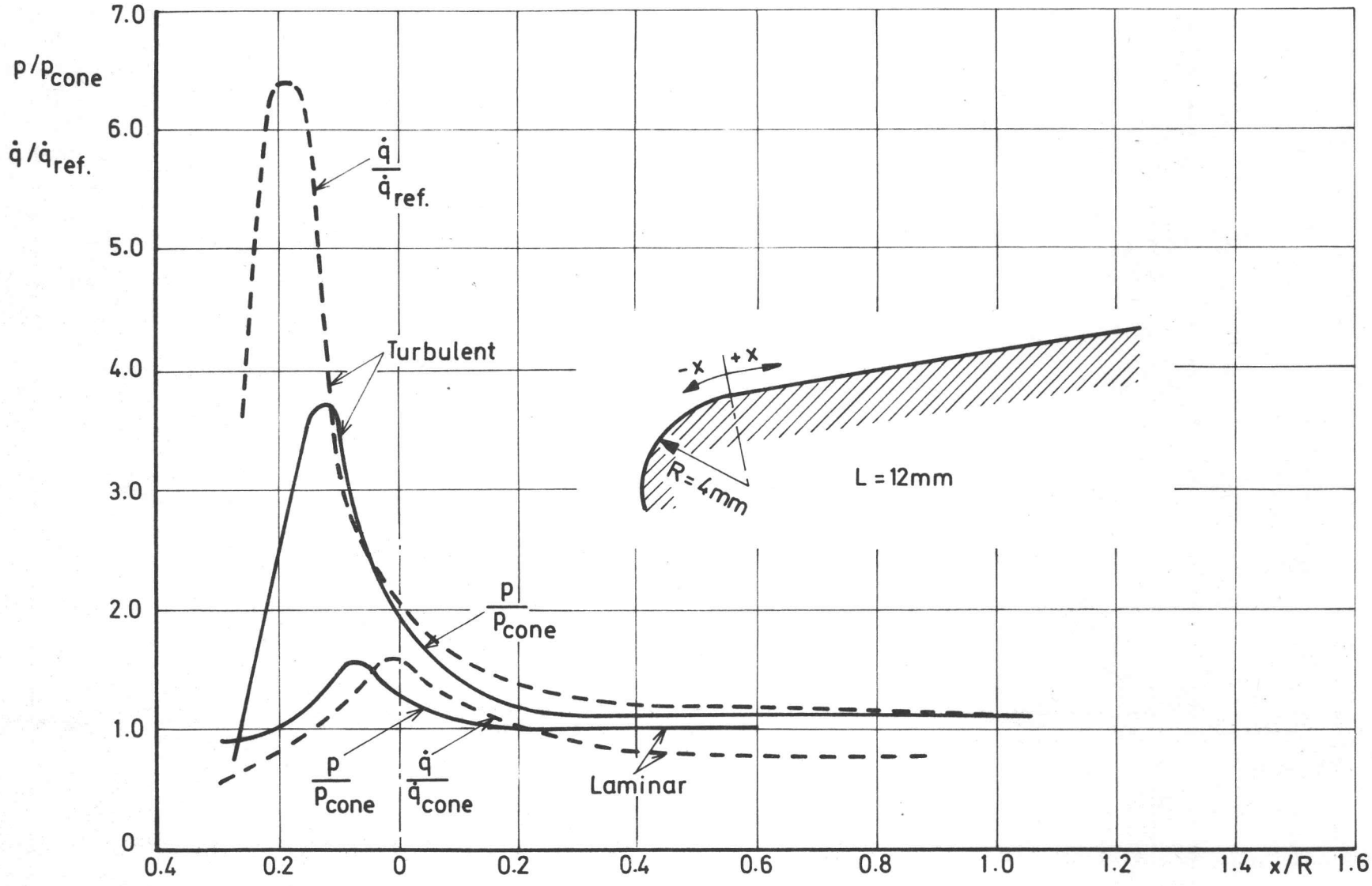

Fig.25- COMPARISON BETWEEN PRESSURE AND HEAT FLUX DISTRIBUTIONS. ZERO INJECTANT MASS FLOW. LAMINAR AND TURBULENT SHEAR LAYER.

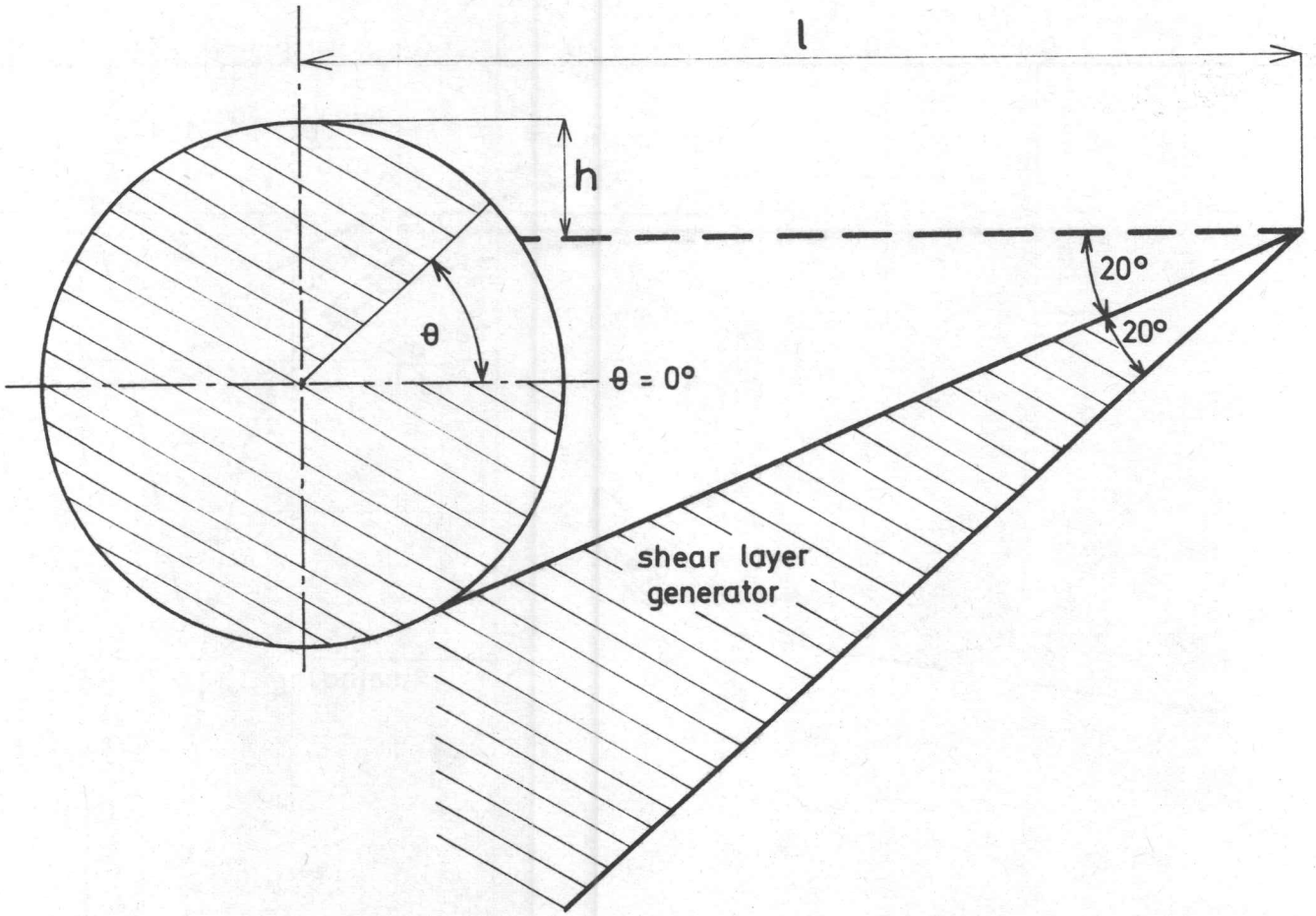

Fig. 26 - DIAGRAM OF CYLINDER AND SHEAR LAYER GENERATOR.

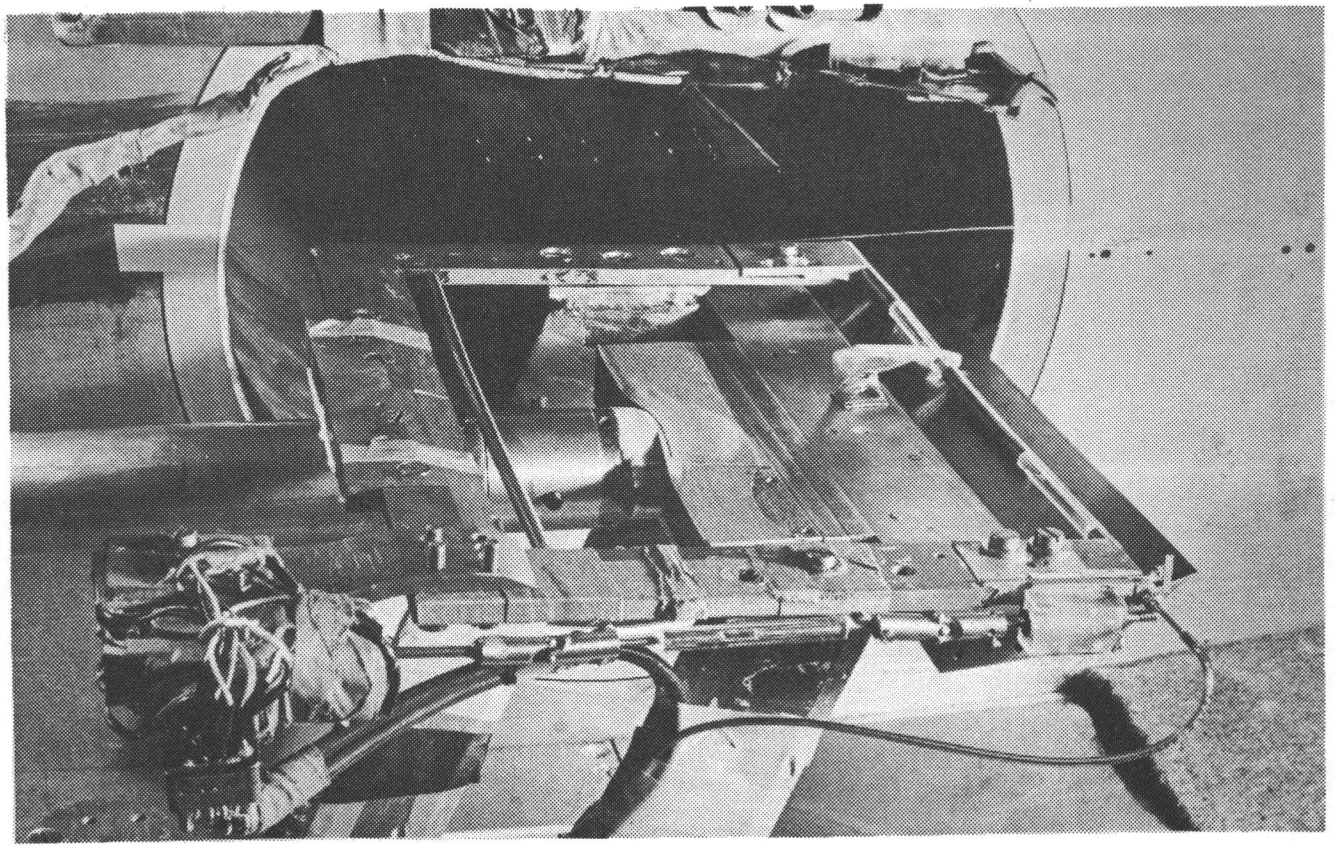

Fig. 27 - EXPERIMENTAL ARRANGEMENT OF THE CYLINDER AND THE SHEAR LAYER GENERATOR.

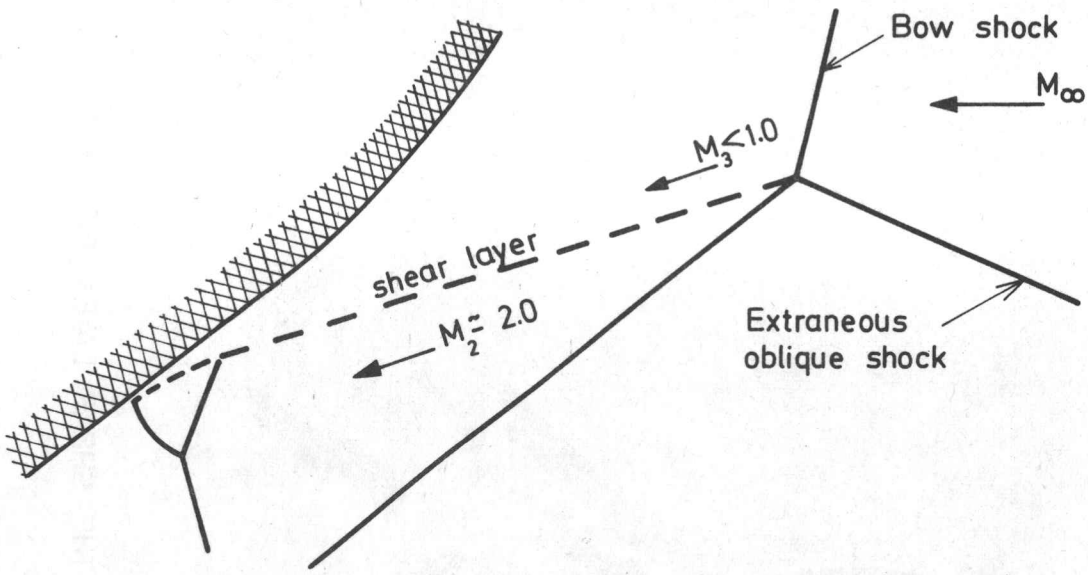

Fig. 28 (a)

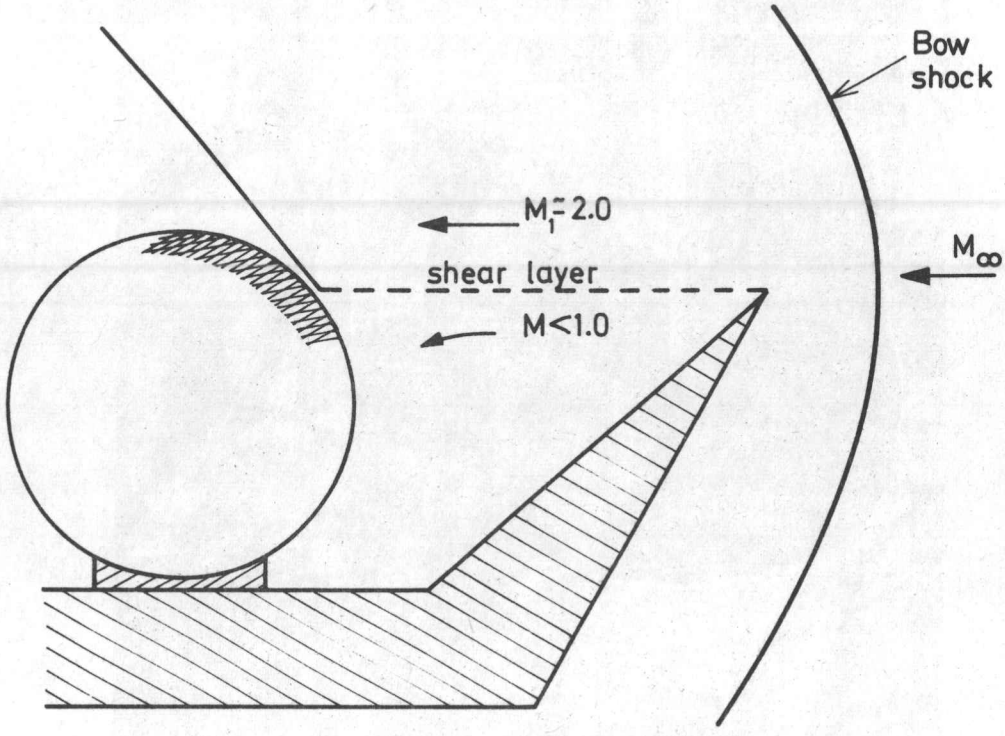

Fig. 28 (b)

Fig. 28 - COMPARISON BETWEEN AN EDNEY TYPE III INTERACTION AND THE EXPERIMENTAL SET UP.

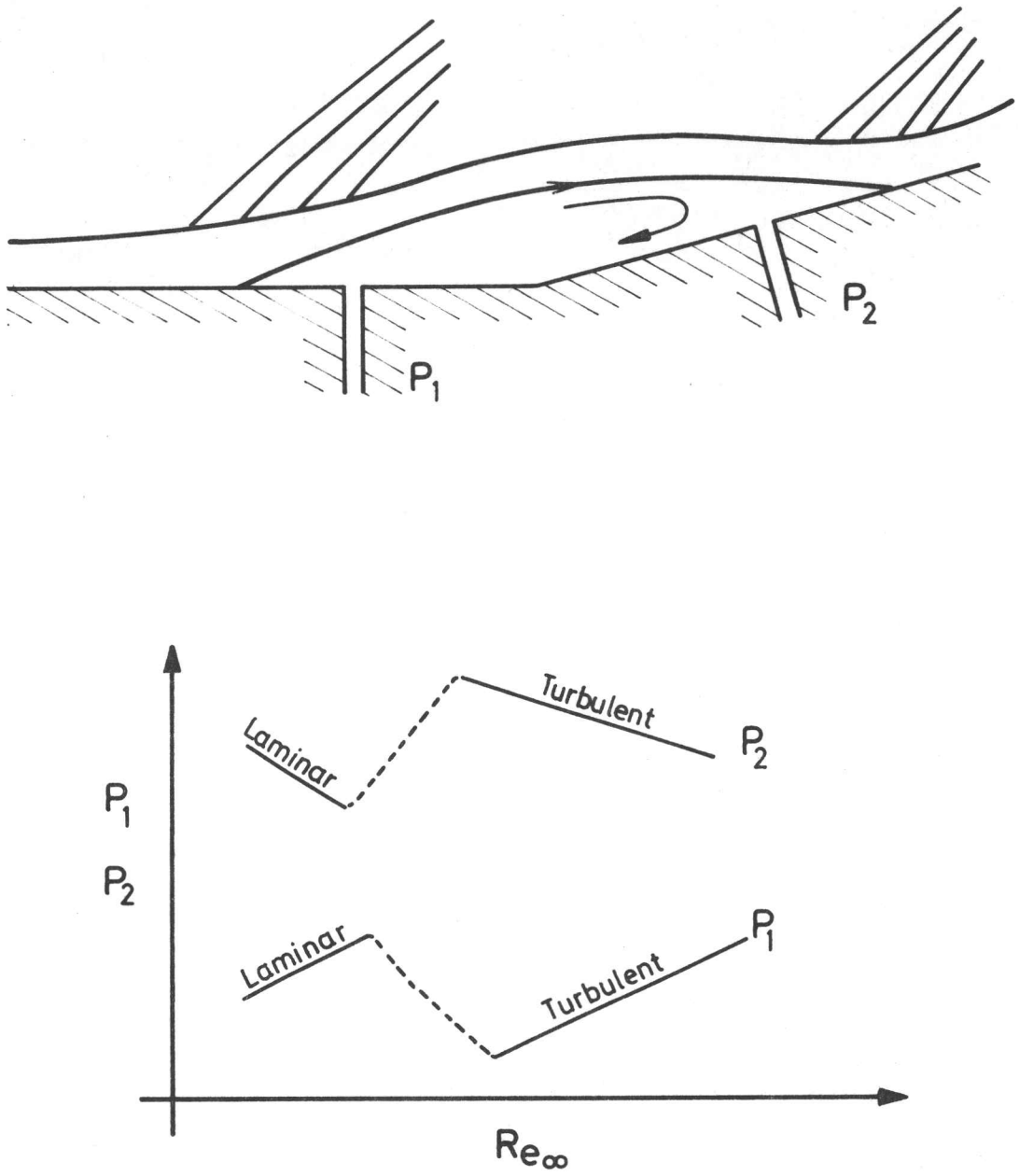

Fig. 29 - DIAGRAMMATIC EXPLANATION OF THE LAMINAR / TURBULENT BOUNDARY LAYER CRITERION.

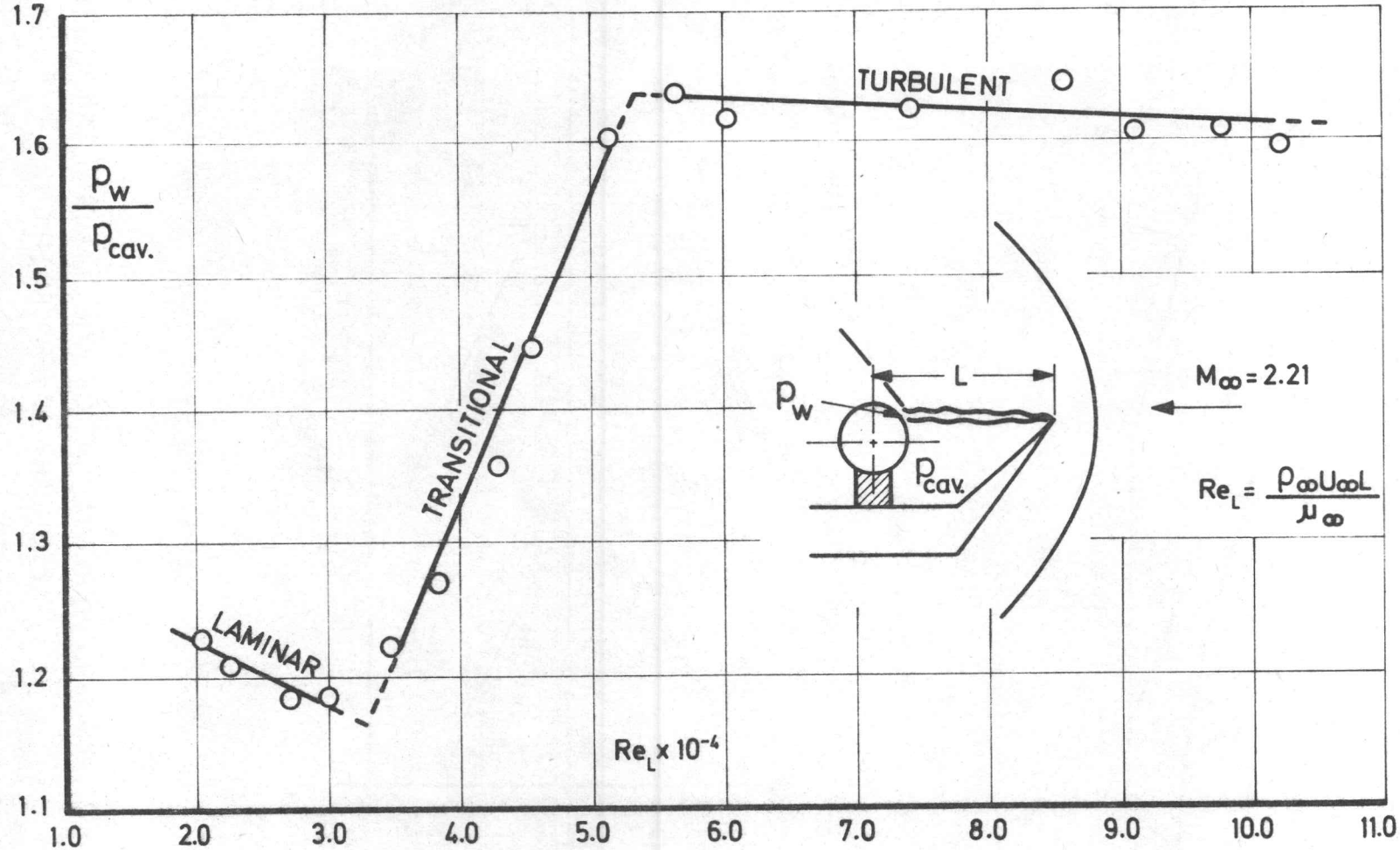

Fig. 30 - FLOW REGIME CRITERION FOR LAMINAR TO TURBULENT SHEAR LAYER.

Fig.31 (a)-LAMINAR

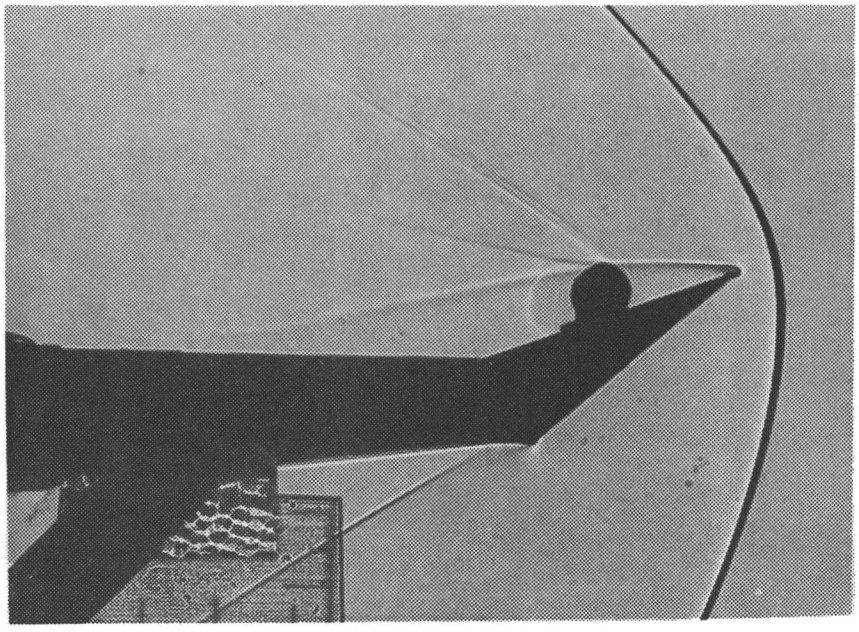

Fig 31 (b)-TURBULENT

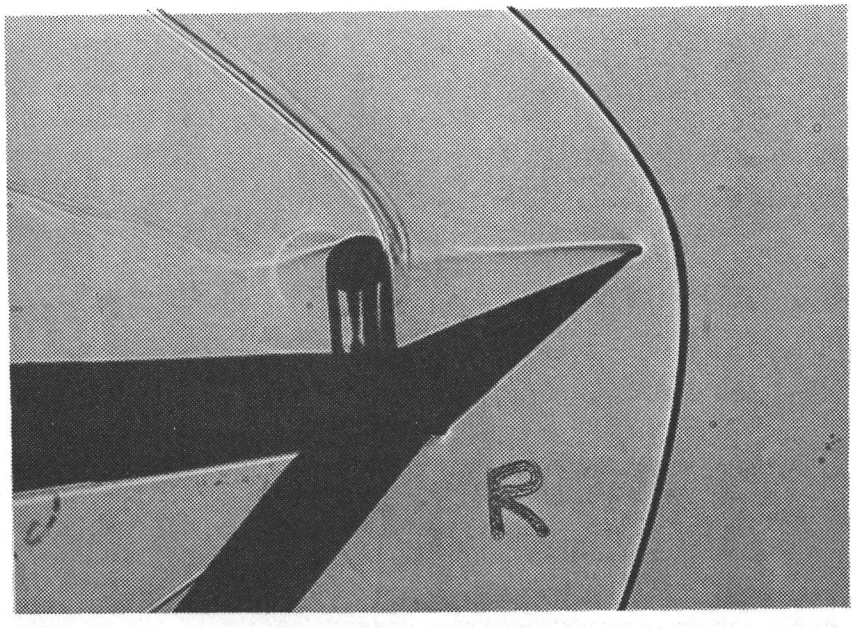

Fig.31 SHADOWGRAPHS OF IMPINGING SHEAR LAYER.

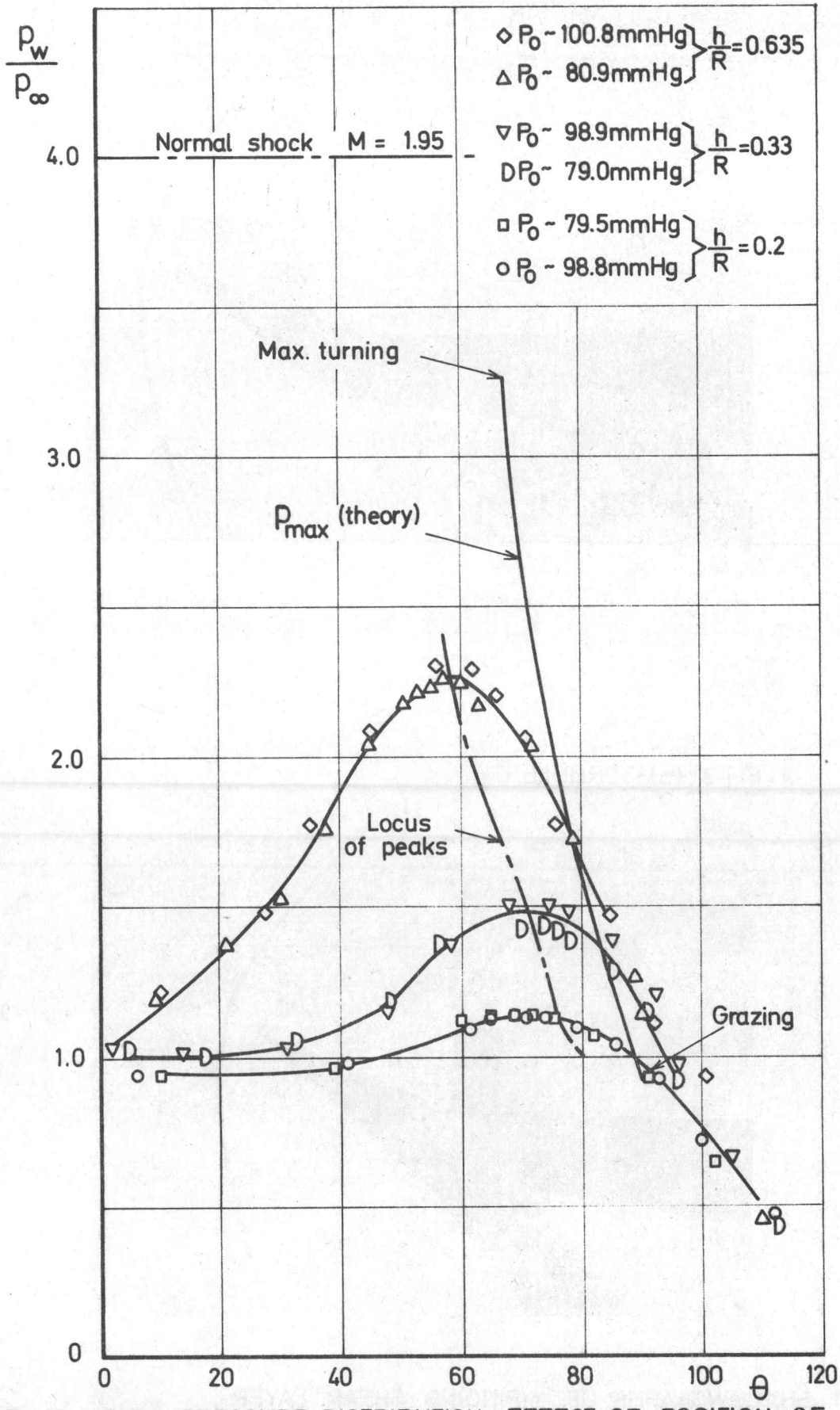

Fig.32 STATIC PRESSURE DISTRIBUTION. EFFECT OF POSITION OF REATTACHMENT POINT. LAMINAR SHEAR LAYER.

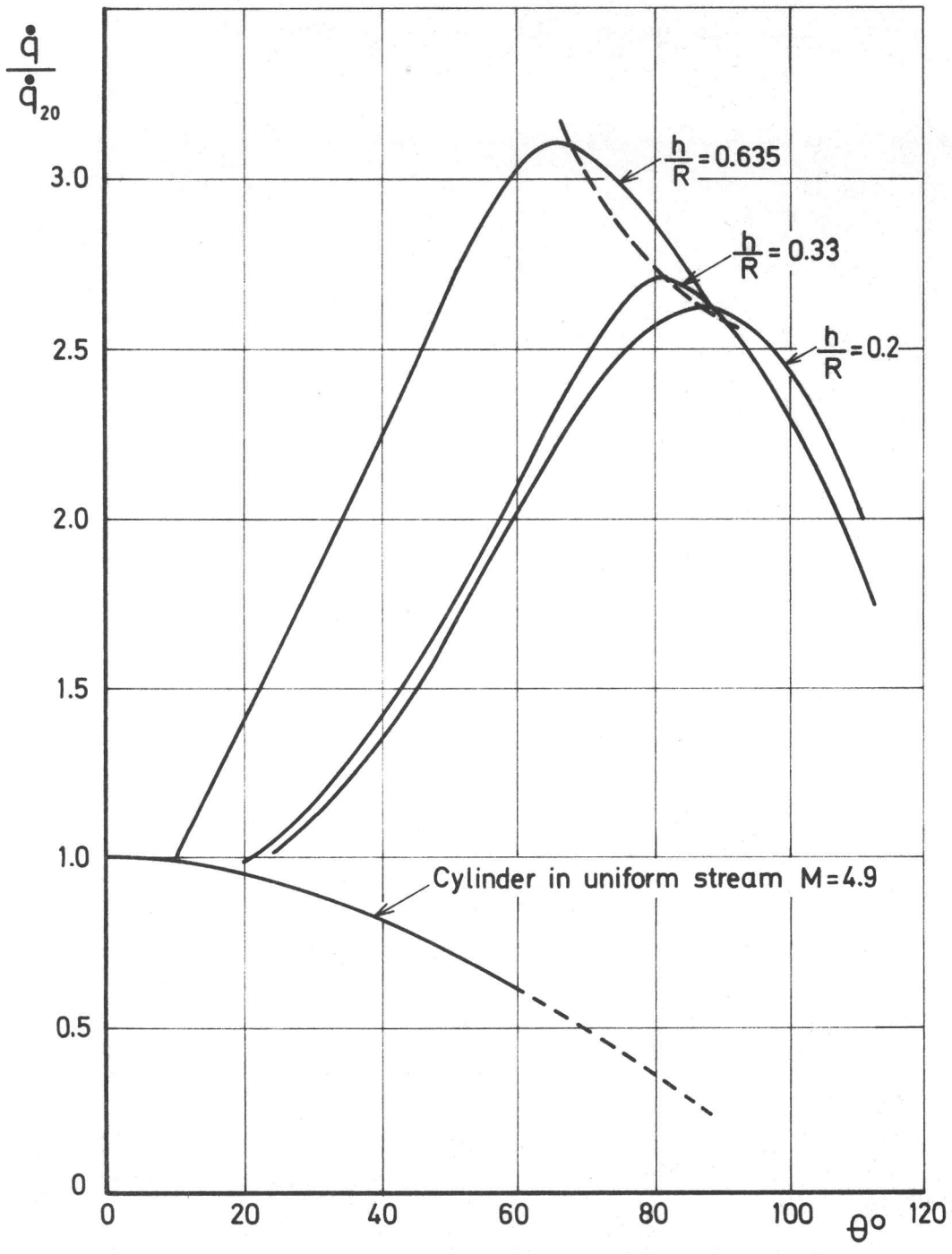

Fig. 33 - HEAT TRANSFER DISTRIBUTIONS. EFFECT OF POSITION OF REATTACHMENT. LAMINAR SHEAR LAYER.

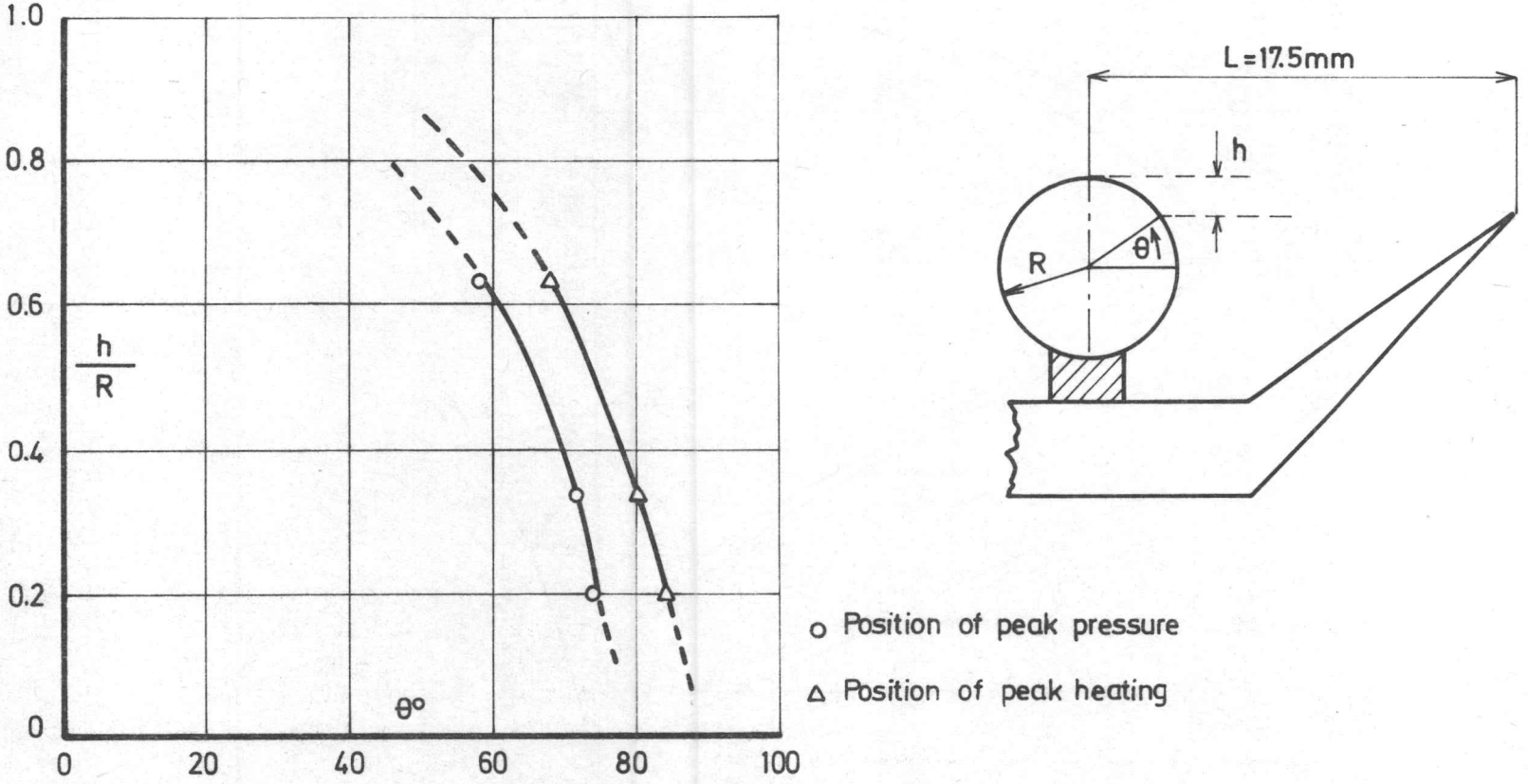

Fig. 34- RELATIVE POSITIONS OF PRESSURE AND HEAT TRANSFER PEAKS. LAMINAR SHEAR LAYER.

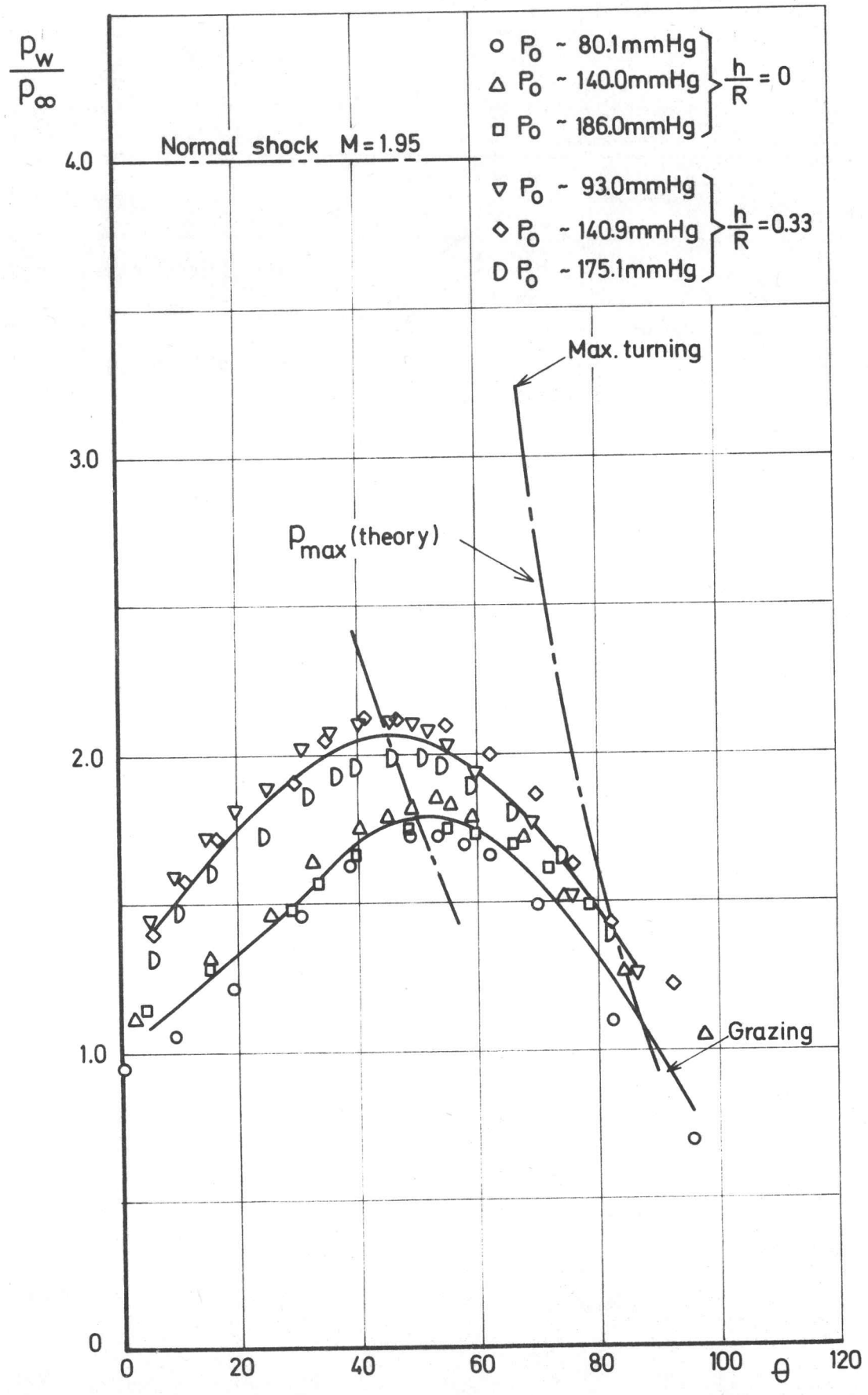

Fig. 35 - STATIC PRESSURE DISTRIBUTION. TURBULENT SHEAR LAYER.

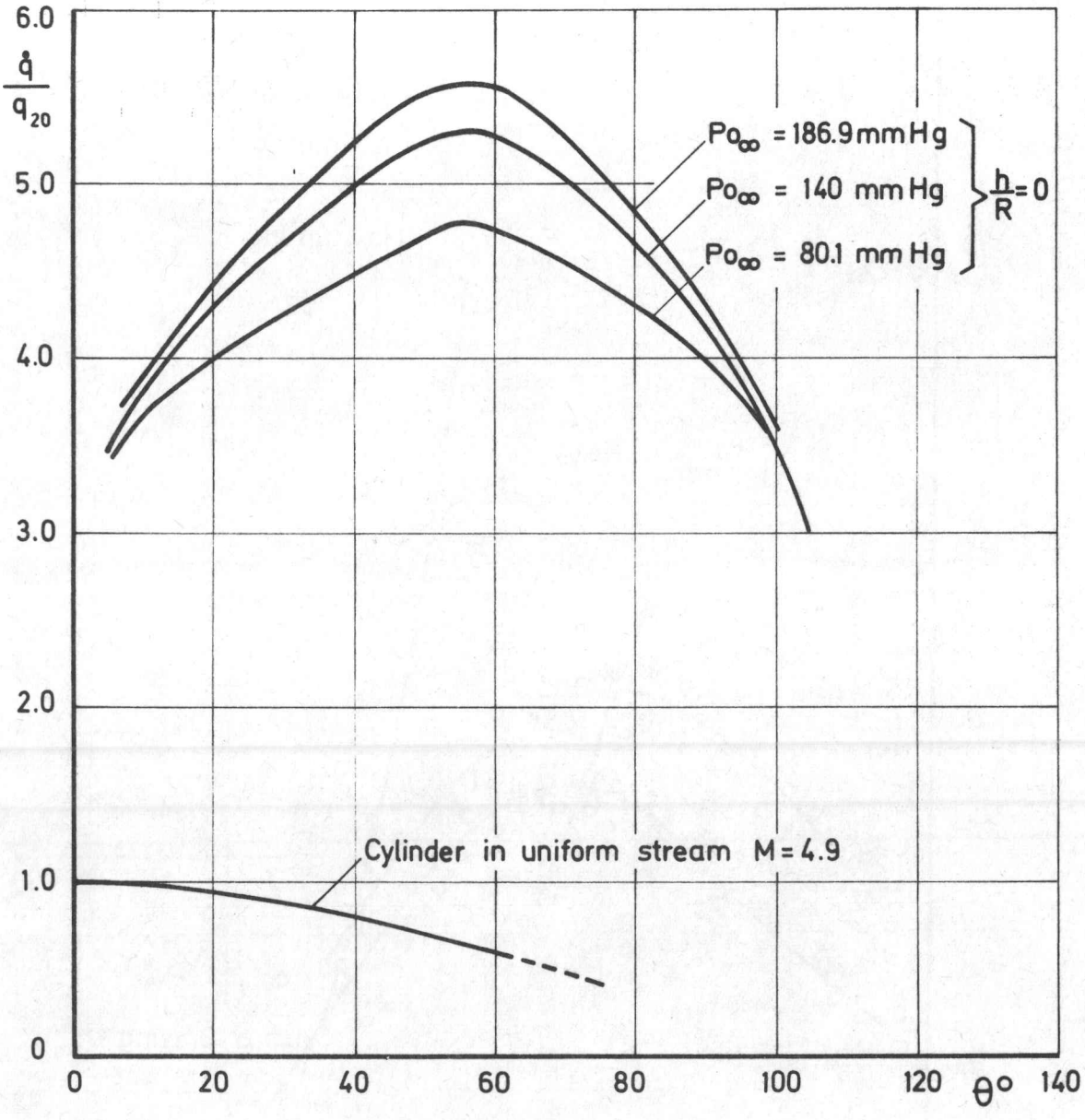

Fig. 36 - HEAT TRANSFER DISTRIBUTION. TURBULENT FLOW.

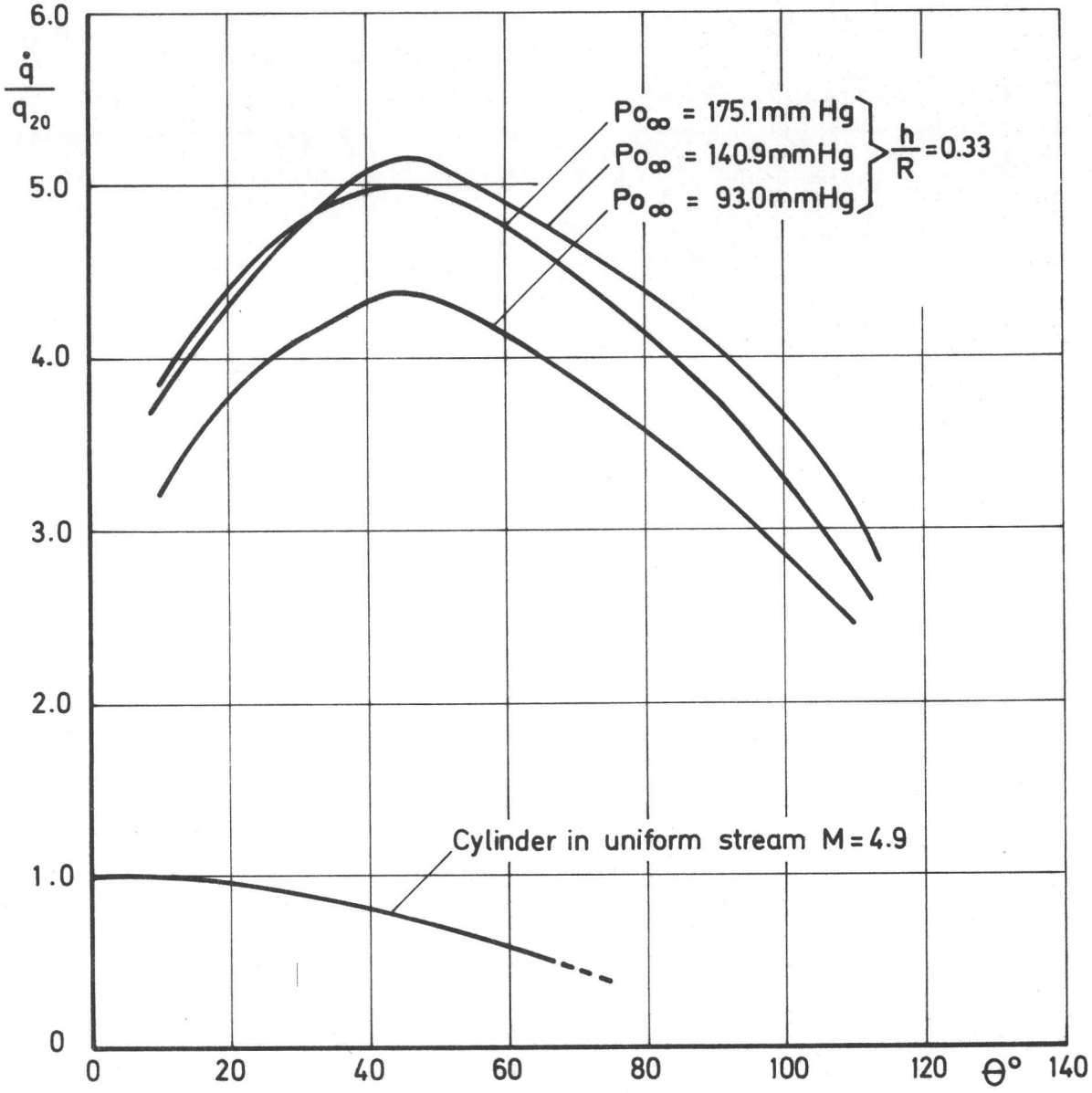

Fig.37 - HEAT TRANSFER DISTRIBUTION. TURBULENT FLOW.

DOCUMENT CONTROL DATA - R&D

(Security classification of title, body of abstract and indexing annotation must be entered when the overall report is classified)

1. Originating Activity (Corporate author) von Karman Institute for Fluid Dynamics High Speed Laboratory	2a. Report Security classification unclassified 2b. Group

3. Report Title

Effect of shock impingement on heat transfer

4. Descriptive notes (type of report and inclusive dates)

Scientific Interim 72 May 01 - 72 December 31

5. Author(s) (Last name, first name, initial)

Ginoux, Jean, J. and Matthews, Richard, D.

6. Report date	7a. Total nº of pages	7b. Nº of refs
30 June 1973	72	29

8a. Contract or grant nº AFOSR 71-2147A b. Project and task nº 9781-02 c. DOD element d. DOD subelement	9a. Originator's report number(s) 9b. Other report nº VKI TN 87

10. Distribution statement

This document has been approved for public release and sale; its distribution is unlimited.

11. Supplementary notes	12. Sponsoring military activity
Tech, other	AF Office of Scientific Research Arlington, Virginia 22209

13. Abstract

The static pressure and heat transfer rate distributions have been measured in the reattachment region of free shear layers. In the first part, a cone/cavity model and the effects of gas injection have been studied. Results are presented for both laminar and turbulent flows.

In the second part, a flow model has been investigated which is analogous with an Edney type III shock wave interaction, found when the bow shock of a blunt hypersonic body is intersected by an extraneous shock.

DD FORM 1473
1 JAN.66

Security classification

KEY WORDS	LINK A		LINK B		LINK C	
	ROLE	WT	ROLE	WT	ROLE	WT
High speed flow						
Shock waves						
Heat transfer						
Shear layers						

Security Classification